

On the estimation of attenuation from the ambient seismic field: inferences from distributions of isotropic point scatterers

Cornelis Weemstra,^{1,*} Roel Snieder² and Lapo Boschi^{3,4}

¹*Institute of Geophysics, ETH, Sonneggstrasse 5, 8092 Zürich, Switzerland. E-mail: kweemstra@gmail.com*

²*Center for Wave Phenomena, Colorado School of Mines, Golden, CO 80401, USA*

³*UPMC, Université Paris 06, ISTEP, F-75005 Paris, France*

⁴*CNRS, UMR 7193, F-75005, Paris, France*

Accepted 2015 July 22. Received 2015 July 22; in original form 2014 July 8

SUMMARY

Cross-correlation of ambient seismic noise recorded by two seismic stations may result in an estimate of the Green's function between those two receivers. Several authors have recently attempted to measure attenuation based on these interferometric, receiver–receiver surface waves. By now, however, it is well established that the loss of coherence of the cross-correlation as a function of space depends strongly on the excitation of the medium. In fact, in a homogeneous dissipative medium, uniform excitation is required to correctly recover attenuation. Applied to fundamental-mode ambient seismic surface waves, this implies that the cross-correlation will decay at the local attenuation rate only if noise sources are distributed uniformly on the Earth's surface. In this study we show that this constraint can be relaxed in case the observed loss of coherence is due to multiple scattering instead of dissipation of energy. We describe the scattering medium as an effective medium whose phase velocity and rate of attenuation are a function of the scatterer density and the average strength of the scatterers. We find that the decay of the cross-correlation in the effective medium coincides with the local attenuation of the effective medium in case the scattering medium is illuminated uniformly from all angles. Consequently, uniform excitation is not a necessary condition for the correct retrieval of scattering attenuation. We exemplify the implications of this finding for studies using the spectrally whitened cross-correlation to infer subsurface attenuation.

Key words: Surface waves and free oscillations; Seismic attenuation; Theoretical seismology; Wave scattering and diffraction.

1 INTRODUCTION

It is now generally accepted that the cross-correlation of recordings made by two receivers is related to (and can in practice be treated as an approximation of) the Green's function at one of these receivers position if there were an impulsive source at the other. The first successful application to the solid Earth is due to Campillo & Paul (2003) who used earthquake coda to obtain empirical Green's functions. Shapiro & Campillo (2004) showed that broad-band Rayleigh waves emerge by simple cross-correlation of continuous recordings of ambient seismic noise. The latter finding holds in media other than the Earth: for example, helioseismology (Duvall *et al.* 1993), underwater acoustics (Roux & Fink 2003), ultrasonics (Weaver & Lobkis 2001, 2002), engineering (Snieder & Şafak 2006; Kohler *et al.* 2007) and infrasound (Haney 2009). Most studies exploiting

the Earth's ambient seismic field use ambient seismic surface wave energy: ocean gravity waves, the main source of ambient seismic noise on Earth, excite surface waves much more effectively than other seismic phases. The process of generating new responses by cross-correlation of ambient seismic signal is often referred to as 'passive seismic interferometry'.

Recently, several researchers have focused on estimating attenuation based on interferometric measurements of surface waves (Prieto *et al.* 2009; Lawrence & Prieto 2011; Lin *et al.* 2011; Weemstra *et al.* 2013). The methodology used in these data studies is based on the derivation of the normalized spatial autocorrelation (SPAC) by Aki (1957). He shows that the SPAC coincides with a zeroth-order Bessel function of the first kind (henceforth Bessel function) in case the medium is illuminated uniformly from all angles. In his derivation Aki assumes a lossless, laterally invariant medium and uncorrelated noise sources. The relation between the SPAC on the one hand and seismic interferometry on the other hand is shown by Yokoi & Margaryan (2008) and Tsai & Moschetti (2010).

*Now at: Department of Geoscience and Engineering, Delft University of Technology, Stevinweg 1, NL-2628 CN Delft, The Netherlands.

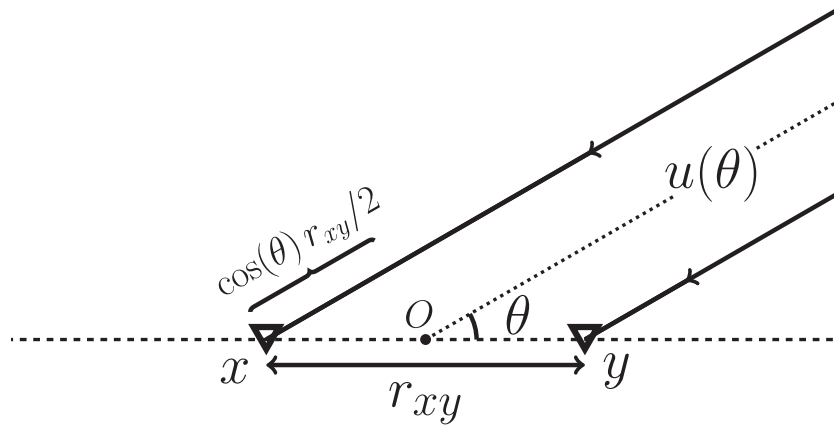


Figure 1. Receivers x and y , along a line with azimuth $\theta = 0$, are separated a distance r_{xy} and equidistant from the origin. The cross-correlation is evaluated for this configuration as function of r_{xy} . The incoming waves are considered plane waves with the amplitude a function of the azimuth.

The Bessel function accounts for loss of coherence due to geometric spreading. In practice, however, ambient surface waves attenuate more due to dissipation of energy and scattering. The interferometric attenuation studies of Prieto *et al.* (2009), Lawrence & Prieto (2011) and Weemstra *et al.* (2013) account for this additional loss of coherence with distance by multiplying the Bessel function with an exponentially decaying term. These authors consider the ‘coherency’, which is defined as the spectrally whitened ensemble (time) averaged cross-spectrum. These authors also average coherency measurements associated with equally separated, but differently oriented receiver couples. Azimuthal averaging of coherency measurements mitigates deviations from the employed model, that is, the exponentially decaying Bessel function, in case of non-uniform illumination patterns (Tsai 2011). Averaging coherency measurements over a multitude of receiver couples comes at a cost however: one implicitly assumes uniform medium properties for the entire study region and hence only a 1-D attenuation profile is obtained (Prieto *et al.* 2009; Weemstra *et al.* 2013). Moreover, violation of this assumption may result in apparent attenuation (Menon *et al.* 2014).

A study by Tsai (2011) suggests that assuming the azimuthally averaged coherency to decay exponentially is contingent upon another assumption, that is that noise sources be uniformly distributed. In fact, his results indicate that different attenuation models should be used for different distributions of sources. Even for radial symmetric distributions of sources, the required model still strongly depends on whether sources are predominantly situated in the far field or in the near field. In his analysis, however, Tsai (2011) confines himself to intrinsic attenuation.

The purpose of this study is to contrast the effect of the two different possible mechanisms of attenuation on the decay of the coherency. That is, we consider the ensemble averaged cross-correlation in a homogeneous dissipative medium (no scattering) and in a lossless scattering medium (no dissipation of energy); analytical treatments are provided in Sections 2 and 3, respectively. In both cases, we restrict ourselves to the two-dimensional (2-D) solution of the wave equation. Interestingly, we find that the model proposed by Prieto *et al.* (2009) correctly explains the decay of the ensemble averaged cross-correlation in case of a lossless scattering medium illuminated uniformly from all angles. In Section 4 we validate numerically the so determined analytical expressions and, additionally, compare the behaviour of the ensemble averaged

cross-correlation in a scattering and dissipative medium for two other illumination patterns. Finally, in Section 5, we present an example that puts our results in perspective.

2 ATTENUATION OF THE AMBIENT SEISMIC FIELD IN A DISSIPATIVE MEDIUM

In this section we analyse the behaviour of the coherency in a homogeneous dissipative medium. For more complex dissipative media we refer to Liu & Ben-Zion (2013). We employ the same formalism as Cox (1973) to describe the cross-spectrum in a 2-D wavefield due to an arbitrary distribution of far-field noise sources. Cross-spectra will be computed in the frequency domain, that is, by multiplication of the reference spectrum with the complex conjugate of the second spectrum. For a single angular frequency ω , the propagation of a plane wave through a dissipative medium can be described by a complex wavenumber \tilde{k} . Physically, the complex wavenumber accounts for dissipation of energy and describes the resulting attenuation. The velocity of the wave is related to the real part of this wavenumber by $c(\omega) = \omega/\Re[\tilde{k}]$. The attenuation coefficient, denoted α , coincides with the imaginary part of \tilde{k} . The wavelength of the attenuated wave is $\lambda \equiv 2\pi c/\omega$.

Similar to Cox (1973), we describe the 2-D noise field by a superposition of plane waves from all azimuths (see also Harmon *et al.* 2010; Tsai 2011); we thus consider sources sufficiently far away compared to the wavelength considered. We evaluate the cross-spectrum along a line centred at the origin and with $\theta = 0$ (Fig. 1). Receivers are defined in pairs along this line: a receiver x in the direction $\theta = \pi$ and a receiver y in the direction $\theta = 0$ and, also by definition, both receivers in a pair are equidistant from the origin and separated by a distance r_{xy} . We consider the incoming signal $u(\theta)$ at the origin, with θ the azimuth from which the signal arrives. We then express phase and amplitude of an incoming signal with respect to that signal’s phase and amplitude at the origin. Consequently, we can write the displacements recorded by receivers x and y immediately in terms of r_{xy} . This is different from formulations where the phase is considered with respect to the source (e.g. Tsai 2011; Boschi *et al.* 2013); in fact, a relocation of the origin would require $u(\theta)$ to change accordingly in our case. In line with our assumption of a homogeneous dissipative medium, phase shifting with respect to the origin implies that we assume \tilde{k} to be constant over the 2-D

space. Integrating the signal arriving from different directions over the azimuth the displacements recorded by x and y are given by,

$$u_x(r_{xy}, \tilde{k}) = \int_0^{2\pi} u(\theta) e^{i\tilde{k} \cos(\theta) r_{xy}/2} d\theta \quad (1)$$

and

$$u_y(r_{xy}, \tilde{k}) = \int_0^{2\pi} u(\theta) e^{-i\tilde{k} \cos(\theta) r_{xy}/2} d\theta, \quad (2)$$

respectively.

We now assume signal from different directions to be uncorrelated, that is, the statistics of the ambient noise field are such that $\langle u(\theta)u^*(\theta') \rangle = |u(\theta)|^2 \delta(\theta - \theta')$; the asterisk denotes complex conjugation. This azimuthal decoherence is in practice exploited by averaging over a sufficiently long time (e.g. Groos & Ritter 2009; Verbeke *et al.* 2012). The ensemble averaged cross-spectrum is given by,

$$\begin{aligned} C^D(r_{xy}, \tilde{k}) &= \langle u_x u_y^* \rangle \\ &= \int_0^{2\pi} \int_0^{2\pi} \langle u(\theta)u^*(\theta') \rangle e^{i(\Re[\tilde{k}] + i\Im[\tilde{k}]) \cos(\theta) r_{xy}/2} \\ &\quad \times e^{i(\Re[\tilde{k}] - i\Im[\tilde{k}]) \cos(\theta') r_{xy}/2} d\theta d\theta' \\ &= \int_0^{2\pi} |u(\theta)|^2 e^{i \cos(\theta) \omega r_{xy}/c} d\theta. \end{aligned} \quad (3)$$

The superscript D signals the incorporation of dissipation of energy in the cross-correlation through the complex wavenumber. This notation allows for an unambiguous comparison with the cross-spectrum affected by scattering (Section 4). Despite the fact that attenuation has been accounted for, C^D is independent of α , which is explained in more detail in Tsai (2011). The independence implies that cross-correlation of far-field sources does not allow for the correct reconstruction of the Green's function between x and y . This can be attributed to the fact that the wave equation for a dissipative medium is not invariant under time-reversal (Snieder *et al.* 2007). Furthermore, we note that the obtained expression depends on the choice of origin, which was observed by Weaver (2012) previously. This dependence casts doubts on the usefulness of the result, but, for our purpose of contrasting attenuation due to scattering with attenuation due to dissipation, is not an obstacle.

Following Cox (1973), we decompose the power of the wavefield in a weighed sum of sines and cosines and introduce the (non-normalized) power density function $P(\theta)$, that is,

$$P(\theta) \equiv |u(\theta)|^2 = \sum_{m=0}^{\infty} [a_m \cos(m\theta) + b_m \sin(m\theta)]. \quad (4)$$

A strongly varying power density function represents a large deviation from a uniform illumination pattern. Substituting eq. (4) in eq. (3), we find,

$$\begin{aligned} C^D(r_{xy}, \tilde{k}) &= \int_0^{2\pi} \sum_{m=0}^{\infty} [a_m \cos(m\theta) + b_m \sin(m\theta)] e^{i \cos(\theta) \omega r_{xy}/c} d\theta \\ &= 2\pi \sum_{m=0}^{\infty} a_m i^m J_m \left(\frac{\omega r_{xy}}{c} \right) \end{aligned} \quad (5)$$

where J_m denotes a Bessel function of the first kind of order m . In the last step we have recognized the Bessel function series [eq. (9.1.21) of Abramowitz & Stegun (1964)]. Since the obtained expression only relies on the a_m , eq. (5) shows explicitly that the cross-correlation is explained by amplitude variations that are symmetric

with respect to $\theta = 0$, that is, with respect to the line connecting the receivers (see also Cox 1973; Harmon *et al.* 2010). In the special case of a uniform power density function, that is, $a_m = 0$ for $m > 0$, C^D is proportional to J_0 , similar to the result of Aki (1957) for a lossless medium. Given cross-correlations computed from an array of receivers, eq. (5) can be used to invert for a truncated series of the Fourier coefficients a_m (Harmon *et al.* 2010).

In recent studies addressing the attenuation of the ambient seismic field, the cross-spectrum is normalized by the product of the root-mean-squares of the two amplitude spectra. As mentioned previously, this physical quantity is generally referred to as the coherency (Prieto *et al.* 2009; Tsai 2011) and the normalization procedure itself as 'spectral whitening'. We define the coherency as

$$\rho_D(r_{xy}, \tilde{k}) \equiv \frac{C^D(r_{xy}, \tilde{k})}{\sqrt{C_{xx}^D(r_{xy}, \tilde{k})} \sqrt{C_{yy}^D(r_{xy}, \tilde{k})}}. \quad (6)$$

We note that Weemstra *et al.* (2014) refer to the normalization in eq. (6) as the 'whitened averaged coherency', which allows them to distinguish it from the case where ensemble averaging takes place after spectral whitening. These authors show that the latter procedure results in a significant amplitude decrease. We emphasize that throughout this work we only consider the procedure in eq. (6), which we will simply refer to as the coherency and which is equivalent to the normalization considered in Tsai (2011) and similar to the normalization used in Prieto *et al.* (2009) and Lawrence & Prieto (2011).

To find a more explicit expression for ρ_D , let us evaluate the terms in the denominator of eq. (6). As shown by Tsai (2011), the ensemble averaged autocorrelation of recordings u_x is given by,

$$\begin{aligned} C_{xx}^D(r_{xy}, \tilde{k}) &= \langle u_x u_x^* \rangle \\ &= \int_0^{2\pi} P(\theta) e^{-\alpha \cos(\theta) r_{xy}} d\theta \\ &= \int_0^{2\pi} \sum_{m=0}^{\infty} [a_m \cos(m\theta) + b_m \sin(m\theta)] e^{-\alpha \cos(\theta) r_{xy}} d\theta \\ &= 2\pi \sum_{m=0}^{\infty} a_m I_m(\alpha r_{xy}) \end{aligned} \quad (7)$$

where I_m denotes a modified Bessel function of the first kind of order m . We have followed the same procedure as in our derivation of C^D and arrive at a summation over integral expressions of the modified Bessel function [eq. (9.6.19) of Abramowitz & Stegun (1964)]. The ensemble averaged autocorrelation of recordings u_y , denoted C_{yy}^D , is obtained in the same way. A slight difference originates from the positive sign in the real exponential term of u_y :

$$C_{yy}^D(r_{xy}, \tilde{k}) = 2\pi \sum_{m=0}^{\infty} (-1)^m a_m I_m(\alpha r_{xy}). \quad (8)$$

Substituting eqs (5), (7) and (8) in expression (6) we recover the result of Tsai (2011), that is,

$$\rho_D(r_{xy}, \tilde{k}) = \frac{\sum_{m=0}^{\infty} a_m i^m J_m(\omega r_{xy}/c)}{\sqrt{\sum_{m=0}^{\infty} a_m I_m(\alpha r_{xy})} \sqrt{\sum_{m=0}^{\infty} (-1)^m a_m I_m(\alpha r_{xy})}}. \quad (9)$$

The behaviour of eq. (9) is discussed in some detail by Tsai (2011) and applies to arbitrary a_m , provided $P(\theta) > 0$ for all θ .

It is useful to note that in case of isotropic illumination (by far-field sources), that is, $a_m = 0$ for $m > 0$ in eq. (4), ρ_D coincides with $[1/I_0(\alpha r_{xy})]J_0(\omega r_{xy}/c)$. This decay is quite different from the behaviour of ρ_D for a homogeneous distribution of sources, that is,

including sources in the near field: in that case it coincides with $e^{-\alpha r_{xy}} J_0(\omega r_{xy}/c)$ (Snieder 2007; Tsai 2011; Nakahara 2012). This difference is exemplary for the dependence of the coherency on the source distribution in case of a dissipative medium, which has been pointed out in detail by Tsai (2011).

Prieto *et al.* (2009) and Lawrence & Prieto (2011) use the exponentially decaying model, that is, $e^{-\alpha r_{xy}} J_0(\omega r_{xy}/c)$, to retrieve surface wave attenuation. To overcome the mapping of azimuthal source distribution variations into the attenuation coefficient these authors average the observed coherency over a set of receiver pairs sampling as many different azimuths as possible. This of course means that only the average attenuation over the area spanned by such receiver pairs can be measured. In the remainder of this study we will refer to this procedure as the ‘exponentially decaying Bessel function method’ and abbreviate it as the ‘EBF method’. Applied to a dissipative medium, azimuthal averaging of coherencies associated with equidistant but differently oriented receiver pairs largely corrects for azimuthal variations in the source distribution (Tsai 2011). For example, the azimuthal average of the coherency computed for an array of receivers illuminated non-uniformly by far-field sources will not be very different from $[1/I_0(\alpha r_{xy})]J_0(\omega r_{xy}/c)$. Importantly, however, azimuthal averaging of the coherency does not correct for variations in source power as a function of distance from the centre of the receiver array: in a dissipative medium sources are still required within the array as well as outside the array to justify the use of $e^{-\alpha r_{xy}} J_0(\omega r_{xy}/c)$ as model.

At the frequencies considered in the studies of Prieto *et al.* (2009) and Lawrence & Prieto (2011), the most notable ambient noise source is forcing by oceanic waves, either direct (Hasselmann 1963) or through non-linear interaction (Longuet-Higgins 1950). Using the EBF method to estimate attenuation may therefore be a good approximation for arrays of receivers at the ocean bottom (e.g. as in Weemstra *et al.* 2013), but expression (9) suggests it is not for arrays of receivers far away from the oceans, for example, central USA. The values found by Prieto *et al.* (2009) and Lawrence & Prieto (2011) for α , however, agree rather well with geology. Especially the attenuation maps produced by Lawrence & Prieto (2011) show anomalies that coincide well with regional tectonic features such as, for example, Yellowstone. At the periods evaluated in this specific study, that is, 24, 12 and 8 s, scattering due to crustal heterogeneities can be significant (Snieder 1988). Surface waves may exhibit significant decay while traveling through such a scattering medium (Foldy 1945; Wu & Aki 1988; Groenenboom & Snieder 1995).

3 ATTENUATION OF THE AMBIENT SEISMIC FIELD IN A SCATTERING MEDIUM

We model a heterogeneous medium by a distribution of isotropic point scatterers. Such scatterers can be thought of as medium heterogeneities represented by single points which, in two dimensions, scatters circular symmetric waves. Assuming an assemblage of isotropic scatterers embedded in a homogeneous and lossless background medium allows for explicit computation of the wavefield (Foldy 1945). At the same time, a wave traveling through an assemblage of isotropic point scatterers can be described by an effective wavenumber whose phase velocity and rate of attenuation depend on (i) the wavenumber of the background medium, (ii) the scatterer density and (iii) the average strength of the scatterers. We note that isotropic point scattering is not essential for the description of

a heterogeneous medium by an effective wavenumber (Lax 1951; Waterman & Truell 1961).

The total wavefield at a location \mathbf{r} can be described as the sum of the background wavefield Ψ_0 and the wavefield due to the scatterers Ψ_s , that is,

$$\Psi(\mathbf{r}) = \Psi_0(\mathbf{r}) + \Psi_s(\mathbf{r}). \quad (10)$$

Since the medium in which the scatterers are embedded is assumed lossless and homogeneous, propagation in this background medium is described by a real wavenumber k_0 . Similarly, the velocity of the background medium is denoted by c_0 and its wavelength by λ_0 . In Appendix A we show how eq. (10) can be written as a linear system of equations in case \mathbf{r} coincides with the location of a scatterer. Solving this linear system of equations for a single incident unit amplitude wave $\Psi_0(\mathbf{r}) \equiv e^{ik_0 \cdot \mathbf{r}}$ enables us to calculate the total wavefield at any location \mathbf{r} . In order to simulate a wavefield consisting of many incoming waves, that is, an assemblage of scatterers illuminated by a diffuse wavefield, the system of equations is solved for each incident wave and the final wavefield at a location \mathbf{r} is simply obtained by summing the individual wavefields at that location. In the next section we present solutions for multiple scattering between isotropic point scatterers for three different background wavefields. For all these solutions, energy is conserved by virtue of the optical theorem.

The amount of energy an incident wavefield loses when impinging on an obstacle is linearly related to the forward scattering amplitude by the optical theorem (van De Hulst 1949; Newton 1976). The relationship was first conceived of by Lord Rayleigh (Strutt 1871). For a 2-D unit amplitude incident wave impinging on an isotropic point scatterer the optical theorem reads (Groenenboom & Snieder 1995):

$$\Omega_{\text{TOT}} = \frac{\Im[f]}{k_0}, \quad (11)$$

where $\Im[f]$ denotes the imaginary part of the scattering amplitude f and Ω_{TOT} the total cross-section. In general, this cross-section represents the loss of energy in the forward direction and hence depends on the wave vector of the incident wave, but, since we consider isotropic point scattering, Ω_{TOT} is independent of the direction of the incident wave in our case. The total cross-section is also often referred to as the extinction cross-section (e.g. Newton 2002).

Removal of energy from the incident wave by a scatterer can be due to two mechanisms: absorption and scattering. The energy loss associated with the absorption is usually referred to as the capture or absorption cross-section, denoted Ω_C and the loss of energy due to scattering is given by the scattering cross-section Ω_S . The total cross-section therefore coincides with the sum of the absorption and scattering cross-section, that is, $\Omega_{\text{TOT}} = \Omega_C + \Omega_S$ (Newton 2002). In this work, we confine ourselves to isotropic point scatterers that do not absorb energy, that is, $\Omega_C = 0$. Conservation of energy therefore equates the total cross-section of a scatterer to its scattering cross-section. We show in Appendix B how this equality enforces a relation between the real and imaginary part of the scattering amplitude: $\Re[f] = \pm \sqrt{-\Im[f](4 + \Im[f])}$. This relation bounds the imaginary part of f and hence caps the maximum scattering amplitude, that is, $-4 \leq \Im[f] \leq 0$ and $|f| \leq 4$. Positive and negative real parts of f correspond to phase advances and phase delays, respectively, and can be loosely interpreted as positive and negative velocity perturbations collapsed to a single point.

Foldy (1945) considers the ensemble averages of the physical quantities of the wavefield, that is, the behaviour of the average over a statistical ensemble of scatterer configurations is evaluated,

henceforth ‘configurational average’. He explicitly derives expressions for the configurational average of the wavefunction, the configurational average of the square of its absolute value and the configurational average of the flux of the wavefunction. The configurational average of the cross-correlation is not treated in Foldy (1945). In this work, we also consider the configurational average of the wavefield and denote it by $\langle \Psi(\mathbf{r}) \rangle$. The configurational average tends to its expected value in the limit of an infinite ensemble of configurations. We will therefore use these terms ‘configurational average’ and ‘expected value’ interchangeably in this study. Also, in the remainder of this work, $\langle \cdot \rangle$ denotes the average over a statistical ensemble of scatterer configurations instead of a statistical ensemble of cross-correlation amplitudes (as was the case in Section 2).

Foldy (1945) shows how the configurational average of the scattered wavefield depends on the scatterer density $\nu(\mathbf{r}, f)$. In this study we assume, for simplicity, the scatterer density as a function of space and the scatterer density as a function of scattering amplitude to be independent. We can therefore drop the dependence of ν on f and account for the dependence of the configurational average on scatterers with varying scatterer amplitudes by introducing the random scattering amplitude F . We denote the corresponding probability density function by p_f : the probability of finding a scatterer with scattering amplitude $F = f$ is given by $p_f(f)$.

Foldy (1945) shows explicitly that $\langle \Psi(\mathbf{r}) \rangle$ satisfies the wave equation with a complex wavenumber k_{eff} . This effective wavenumber depends on the wavenumber of the background medium, that is, k_0 , plus an additional term depending on ν and F . In two dimensions we have (Groenenboom & Snieder 1995),

$$k_{\text{eff}}(\mathbf{r}) = k_0 \sqrt{1 - \frac{\nu(F)}{k_0^2}}, \quad (12)$$

where the spatial dependence stems from the spatial variation of ν . Substituting k_{eff} for k_0 in eq. (A1) essentially dampens the background wavefield and retards/advances its phase (depending on the sign of $\Re[f]$ in eq. (B3)). Similar to \tilde{k} in Section 2, the phase velocity and attenuation coefficient of the configurationally averaged scattered wavefield are given by

$$c = \frac{\omega}{\Re[k_{\text{eff}}]} \quad (13)$$

and

$$\alpha = \Im[k_{\text{eff}}], \quad (14)$$

respectively. We obtain k_{eff} by taking the principal square root in eq. (12) since that is the only square root with a physical meaning, that is, corresponding to $\alpha > 0$. Note that because both k_0 and ν can be expressed in terms of λ_0 , also k_{eff} (and hence α) can be expressed in terms of λ_0 . In the next section we therefore express all relevant variables (ν , k_{eff} , α , receiver separation, etc.) in terms of λ_0 .

Provided the scatterer density and the expected value of the random scattering amplitude are known, eq. (12) can be used to compute the expected attenuation and phase delay due to an assemblage of isotropic point scatterers. The expected value of the random scattering amplitude is, by definition, given by

$$\langle F \rangle = \int p_f(f) f df, \quad (15)$$

where integration is over all values of f for which $\Re[f] = \pm \sqrt{-\Im[f](4 + \Im[f])}$. In the next section we consider the simplest case of scatterers with equal amplitudes f_0 . This assumption implies that $p_f = \delta(f - f_0)$, where δ is the Dirac delta function and hence $\langle F \rangle = f_0$. In Section 5, however, we allow for scatterers with

varying scattering amplitudes by setting p_f equal to a raised cosine distribution.

In order to compare the behaviour of the ensemble averaged cross-spectrum and the coherency in a scattered wavefield to the analytical expressions obtained in Section 2, we introduce the counterparts of these expressions in the scattered wavefield. These counterparts are computed using displacements, that is, $\Psi(\mathbf{r})$, obtained from solutions of the multiple scattering inverse problem. The cross-spectrum associated with a single scattering realization, denoted C^S , is defined as

$$C^S(r_{xy}) \equiv \Psi_x \Psi_y^*, \quad (16)$$

where Ψ_x and Ψ_y are the displacements at the locations of receivers x and y , respectively. Since $\Psi = \Psi_0 + \Psi_S$, the cross-correlation of the direct wave can be isolated: it is simply obtained by multiplication of Ψ_0 measured by receiver x with the complex conjugate of Ψ_0 measured by receiver y . We denote this measurable C_0^S and, additionally, define the complementary part $C_s^S \equiv C^S - C_0^S$. This complementary part includes correlations between the direct wave and the scattered waves and mutual correlations between the scattered waves. In fact, for a single incident wave, C_s^S contains many of these ‘spurious arrivals’ (see Snieder & Fleury (2010) for a theoretical explanation and Godin *et al.* (2010) for observations of spurious arrivals). The coherency in the scattered wavefield, denoted ρ_S , is defined as

$$\rho_S(r_{xy}) \equiv \frac{C^S(r_{xy})}{\sqrt{C_{xx}^S} \sqrt{C_{yy}^S}}. \quad (17)$$

An overview of the symbols associated with the different physical quantities is given in Table 1.

We consider a wavefield due to an assemblage of point scatterers embedded in a lossless background medium. Similar to the dissipative medium considered in Section 2, we consider the scattering medium to be illuminated uniformly from all angles by far-field sources. For this specific case, Wapenaar & Fokkema (2006) show that the cross-spectrum between any two points in the scattering medium is inversely proportional to the imaginary part of the Green’s function between those two points, that is,

$$C^S(r_{xy}) \propto -\Im[G(r_{xy})]. \quad (18)$$

Since this relation (18) holds for arbitrary medium properties, $G(r_{xy})$ contains both the direct wave between y and x , denoted by $G^{(0)}(r_{xy})$ and scattering contributions. Note that in the absence of scatterers, $G^{(0)}(r_{xy})$ can be substituted in (18) and, using eq. (A3), we have $C^S(r_{xy}) = C_0^S \propto J_0(k_0 r_{xy})$.

We recall that Foldy (1945) shows explicitly that $\langle \Psi(\mathbf{r}) \rangle$ satisfies the wave equation with a complex wavenumber k_{eff} . Consequently, for a homogeneous effective medium, that is, constant k_{eff} , the Green’s function is given by,

$$\langle G(r_{xy}) \rangle = \frac{-i}{4} H_0^{(2)}(k_{\text{eff}} r_{xy}) \quad (19)$$

which upon substitution of the right-hand side of expression (12) can be written as

$$\langle G(r_{xy}) \rangle = \frac{-i}{4} H_0^{(2)} \left(\sqrt{k_0^2 - \Re[\nu(F)]} - i \Im[\nu(F)] \times r_{xy} \right). \quad (20)$$

Tsai (2011) notes that the Hankel function with a complex argument can, for $b \ll a$, be approximated as follows,

$$H_0^{(2)} \left(a r_{xy} \sqrt{1 + \frac{ib}{a}} \right) \approx H_0^{(2)}(a r_{xy}) e^{-br_{xy}/2}. \quad (21)$$

Table 1. Symbols for the different physical quantities.

Symbol	Explanation
Ψ	Scattered wavefield
Ψ_0	Background wavefield
Ψ_s	Wavefield due to scatterers ($\Psi - \Psi_0$)
C^D	Cross-spectrum in a dissipative medium (propagation described by \tilde{k})
C^S	Cross-spectrum in a scattering medium
C_0^S	Cross-spectrum of the background wavefield in the scattering medium
C_s^S	The part of the cross-spectrum due to the presence of the scatterers ($C^S - C_0^S$)
ρ_D	Coherency in a dissipative medium (eq. 9)
ρ_S	Coherency in a scattering medium (eq. 17)

Adapted to the argument of the Hankel function in eq. (20) this gives $a = \sqrt{k_0^2 - \Re[v(F)]}$, $b = -\Im[v(F)]/\sqrt{k_0^2 - \Re[v(F)]}$ and the approximation holds for $-\Im[v(F)] \ll k_0^2 - \Re[v(F)]$ (note that $-\Im[v(F)] > 0$ because $\Im[f] < 0$ for all f and v is real). Substituting the approximation for the Hankel function in expression (20) yields

$$\langle G(r_{xy}) \rangle \approx \frac{-i}{4} H_0^{(2)} \left[\sqrt{k_0^2 - \Re[v(F)]} \times r_{xy} \right] e^{-\alpha r_{xy}}, \quad (22)$$

where, according to (21), α is approximated by,

$$\alpha \approx \frac{-\Im[v(F)]}{2\sqrt{k_0^2 - \Re[v(F)]}}. \quad (23)$$

Note that the right-hand side expression hence approximates $\Im[k_{\text{eff}}]$. Similarly, c is approximated by

$$c \approx \frac{\omega}{\sqrt{k_0^2 - \Re[v(F)]}}, \quad (24)$$

whose denominator approximates $\Re[k_{\text{eff}}]$. We note that these approximations for c and α can also be inferred directly from eq. (12): a complex number z with a real and imaginary part that are both positive and for which the imaginary part is small with respect to its real part, that is, $\Im[z] \ll \Re[z]$, has a principal square root that can be approximated by $\sqrt{z} \approx \sqrt{\Re[z]} + i\Im[z]/(2\sqrt{\Re[z]})$.

We now draw a connection between relation (18) and eq. (22). Although $G(r_{xy})$ includes both the direct wave and scattered waves between receivers x and y , Foldy's result implies that its expected value can be approximated by eq. (22). Specifically, the imaginary part of this approximation behaves like $-J_0 \left(\sqrt{k_0^2 - \Re[v(F)]} r_{xy} \right) e^{-\alpha r_{xy}}$.

For isotropic illumination, relation (18) tells us that $C^S(r_{xy})$ and $\Im[G(r_{xy})]$ are inversely proportional and hence so are $\langle C^S(r_{xy}) \rangle$ and $\langle \Im[G(r_{xy})] \rangle$. Consequently, we can conclude that,

$$\langle C^S(r_{xy}) \rangle \propto J_0 \left(\frac{\omega r_{xy}}{c} \right) e^{-\alpha r_{xy}}, \quad (25)$$

where c and α are given by eqs (24) and (23), respectively.

Summarizing the above, consider an (expected) wavefield in a lossless scattering medium with a uniform scatterer density described by k_{eff} and another wavefield in a homogeneous dissipative medium described by \tilde{k} . Furthermore, assume both wavenumbers to coincide, that is, $k_{\text{eff}} = \tilde{k}$. The latter implies that the velocity and attenuation of a plane wave traveling through the dissipative medium will coincide with the (expected) velocity and attenuation of a plane wave propagating through the scattering medium. However, in case the same two media are illuminated uniformly from all angles by mutual uncorrelated noise sources located in the far field, the cross-spectrum in the scattering medium can be expected

to decay exponentially with distance, whereas the cross-spectrum in the dissipative medium does not decay at all (eq. 5 with $a_m = 0$ for $m > 0$). This difference between $\langle C^S(r_{xy}) \rangle$ and $C^D(r_{xy})$ is confirmed by the numerical experiments in the next section.

4 NUMERICAL SIMULATIONS

We numerically investigate the cross-spectrum in a medium populated with isotropic point scatterers for three different illumination patterns. For each illumination pattern $P(\theta)$, we compare the configurationally averaged cross-spectrum in the scattering medium to the cross-spectrum in a dissipative medium whose wavefield is described by the same wavenumber, that is, we consider $\tilde{k} = k_{\text{eff}}$. Throughout this section, we express all relevant parameters and variables in terms of λ_0 . In all three experiments we consider a total of four thousand ($N = 4000$) scatterers which we randomly place within a circle with radius $R = 20\lambda_0$ (Fig. 2); this implies a constant $\nu = 4000/(\pi 20^2 \lambda_0^2)$. We consider an attenuation rate of $\alpha = 0.075/\lambda_0$, which upon inversion of eq. (12) yields $\langle F \rangle = f_0 \approx -1.067 - 0.309i$ and implies $k_{\text{eff}} = (6.548 + 0.075i)/\lambda_0$. Note that a phase delay of the average wavefield is imposed by prescribing $\Re[f_0] < 0$. Under these assumptions, the rate of attenuation and relative phase velocity decrease of the configurationally averaged wavefield are constant throughout the scattering medium. Fig. 3 presents the rate of attenuation and relative phase velocity decrease as a function of ν and $\Im[F]$. The considered attenuation rate of $\alpha = 0.075/\lambda_0$ represents, for example, a surface wave with a period of 8 s traveling with a background velocity of 3 km s⁻¹ whose of attenuation is described by an attenuation coefficient of $3.125 \times 10^{-3} \text{ km}^{-1}$.

Consistent with our derivation in Section 2, we also assumed plane waves in Section 3: k_{eff} describes a damped and phase retarded/advanced plane wave (eq. 12). Recall from Section 3 that the scatterers are embedded in a lossless and homogeneous background medium in which the propagation is described by a real wavenumber k_0 (and its velocity and wavelength by c_0 and λ_0 , respectively). In practice, an incident plane wave is modeled by a far-field impulsive source at a distance of $333.3\lambda_0$ from the origin; its signature is therefore given by eq. (A3). Since we consider a total of 4000 scatterers, numerical modeling involves solving a system of 4000 equations for each of these sources (see Appendix A). The wavefield due to the scatterers $\Psi_s(\mathbf{r})$ at any location \mathbf{r} can subsequently be obtained by substituting the obtained solutions for the $\Psi(\mathbf{r}_j)$ in eq. (A2). Finally, the total wavefield $\Psi(\mathbf{r})$ results from a simple summation of the background wavefield, $\Psi_0(\mathbf{r})$ and the wavefield due to the scatterers, $\Psi_s(\mathbf{r})$ (eq. 10). In Section 2 we explicitly assumed simultaneously acting uncorrelated sources. We showed in eq. (3) that this azimuthal decoherence reduces the calculation of the ensemble-averaged cross-correlation to a single integral. In

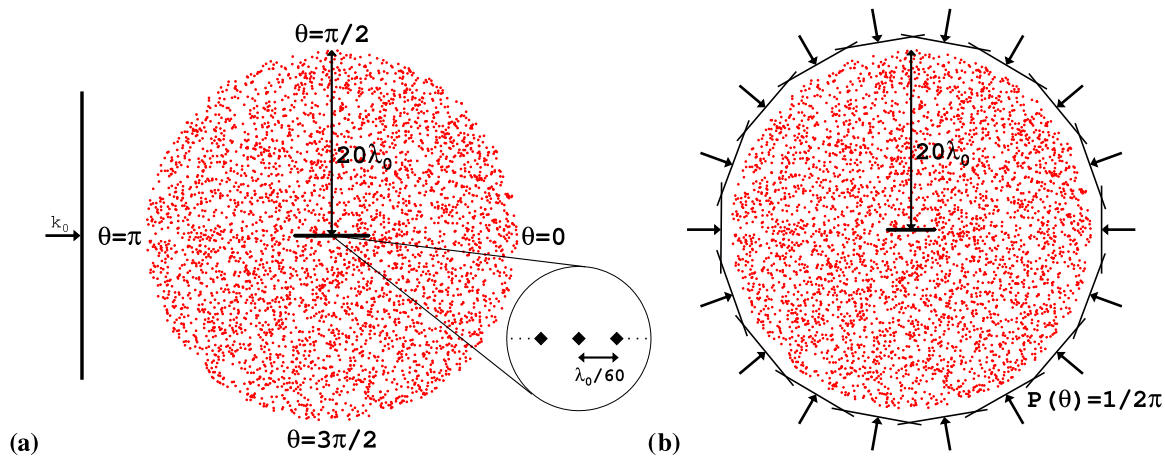


Figure 2. The experimental setup of the first (a) and second experiment (b). Red dots represent (a single scattering realization of) isotropic point scatterers. In our first experiment we consider a single incident plane wave from a direction $\theta = \pi$ while in the second experiment we prescribe a uniform distribution of far-field sources, that is, uniform $P(\theta)$. A zoom-in on the very centre of (a) depicts the receivers as black diamonds separated by $\lambda_0/60$.

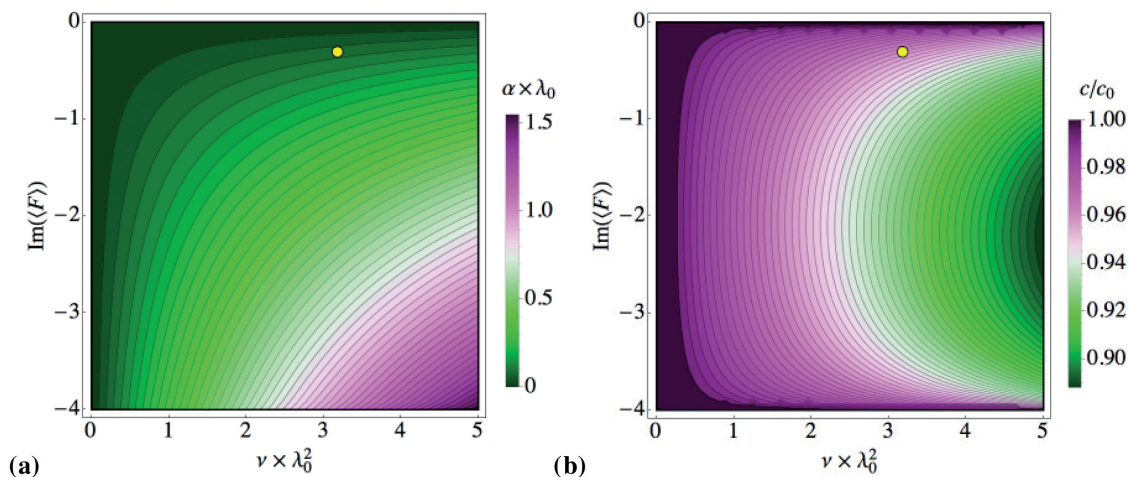


Figure 3. Attenuation coefficient (a) and relative phase velocity decrease (b) of the configurationally averaged wave as a function of scatterer density and the imaginary part of the scattering amplitude. A yellow dot marks the scatterer density and imaginary part of the scattering amplitude associated with the expected attenuation and relative phase velocity decrease considered in this section. Note that we have prescribed the real part of the scattering amplitude to be negative.

all our numerical experiments (both in this section and the next section), we will assume this azimuthal decoherence. This implies that for any superposition of plane waves, that is, any $P(\theta)$, we compute cross-spectra individually for each incident wave (including scattering events) and subsequently stack them.

The configurational average of the physical quantities of interest, that is, Ψ , C^S and ρ_S , is computed by averaging over a total of M ‘scattering realizations’; each realization associated with a (different) random configuration of the scatterers. We consider three different experiments which are discriminated from each other by their illumination of the line of receivers, that is, by $P(\theta)$. The order in which we conduct these experiments serves to incrementally increase our understanding. In the first experiment we consider a single plane wave impinging on the distributions of scatterers, subsequently we examine the effect of a uniform $P(\theta)$ and, finally, we investigate the behaviour of the cross-spectrum in case of some random illumination function.

4.1 Experiment 1: a single plane wave

We consider a single incident plane wave illuminating the distribution of scatterers from the azimuth $\theta = \pi$ (Fig. 2a). The spectrum

$[\Psi(r)$; see eq. (10)] is computed at 481 locations (240 receivers x , 240 receivers y and one at the centre) where the distance between neighboring receivers is $\lambda_0/60$. The configurationally averaged wavefield is obtained by averaging over a total of 38 400 scattering realizations. The spectrum associated with a single scattering realization is shown, as function of location along the line of receivers, in Fig. 4(a) (realization no. 30001; chosen arbitrarily). In the same graph, the configurationally averaged wavefield is plotted (i.e. the wave described by k_{eff}). It is clear that the impact of the isotropic point scatterers is such that the spectrum associated with a single realization by no means approximates the configurationally averaged wave. In Fig. 4(b) we separate the contributions of Ψ_0 and Ψ_s (see Appendix A for details). This shows that the direct wave has a significantly lower amplitude than the signal due to the combined effect of the scatterers. Finally, Fig. 4(c) shows the configurationally averaged wavefield. The numerically obtained $\langle \Psi \rangle$ coincides with the predicted (analytical) configurational average, that is, with the wave propagating with wavenumber k_{eff} . This confirms that our setup enables us to successfully simulate the configurationally averaged wavefield. The increasing phase delay and decreasing amplitude with respect to the direct wave is the (average) signature of the isotropic point scatterers. The decrease in amplitude

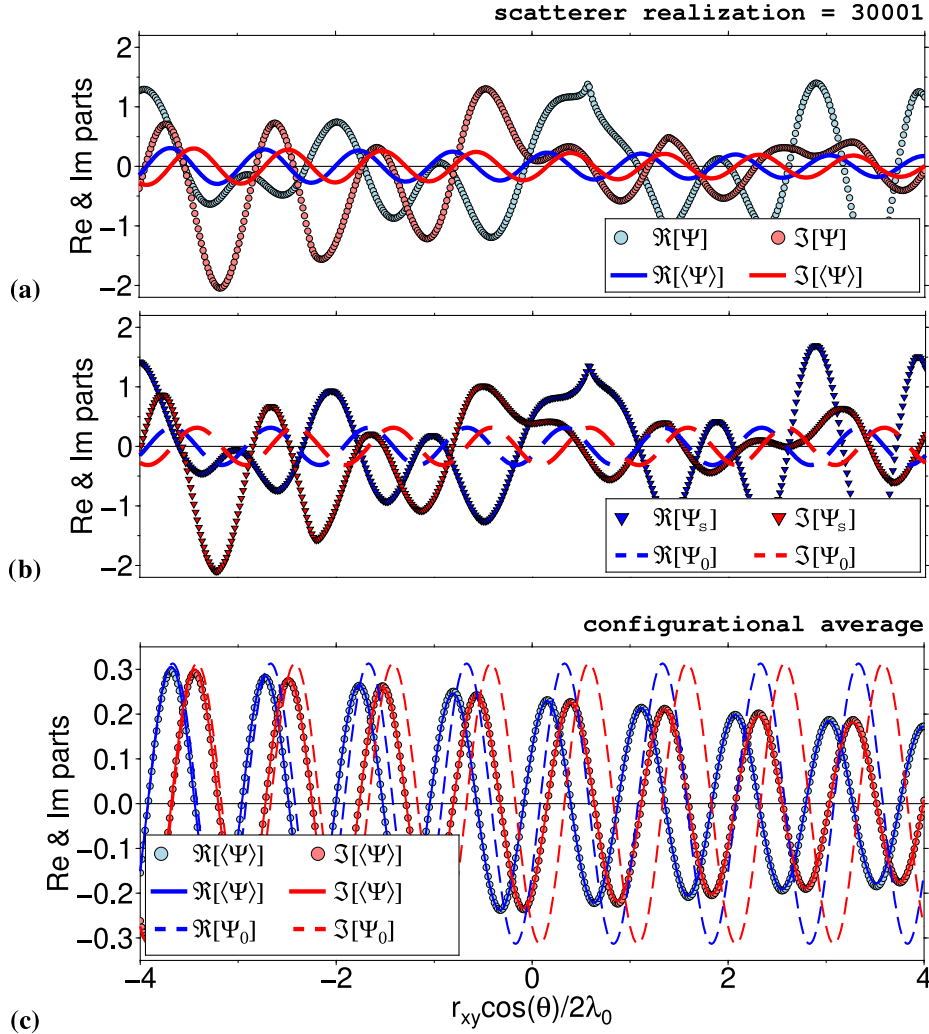


Figure 4. Experiment 1: the spectrum as a function of distance in the scattered wavefield. The spectrum associated with a single configuration of the scatterers (Ψ) is presented in (a). The light blue and red dots depict the real and imaginary part of the spectrum, respectively. The solid blue and red lines represent the real and imaginary part of the configurationally averaged wavefield, that is, $\langle\Psi\rangle$, respectively. The contributions of the direct wave (Ψ_0 ; dashed line) and the wavefield due to the scatterers (Ψ_s ; triangles) are separated in (b). The bottom graph (c) shows the configurationally averaged wavefield obtained from our numerical experiment (dots) and predicted by Foldy (1945), that is, k_{eff} (solid lines). Also, the direct, non-attenuated wave, is plotted (dashed lines).

is predominantly due to the ‘randomization’ of the wavefield (Wu 1982).

The cross-spectrum of the scattering realization presented in Fig. 4 is shown in Fig. 5(a). We only compute cross-spectra for receivers equidistant from the origin, r_{xy} is hence incremented by $\lambda_0/30$. The strong fluctuations in the spectrum cause the cross-spectrum to behave very different from the cross-spectrum of the direct wave (Fig. 5b), where we have normalized both $C_0^S(r_{xy})$ and $C_s^S(r_{xy})$ with respect to $C_0^S(r_{xy} = 0)$. This shows explicitly (for the considered scatterer density and strength) that the wavefield due to the scatterers has an impact on the cross-correlation that is more than an order of magnitude larger than the cross-spectrum of the direct wave. In the time domain this manifests itself as high amplitude seismic coda (Groenenboom & Snieder 1995). These coda can be used to retrieve the Green’s function between a pair of receivers (Campillo & Paul 2003; Snieder 2004). Since the ambient seismic field is a combination of direct arrivals and scattered waves, however, we do not aim to separate their effect in this study (note that splitting C^S in C_0^S and C_s^S is not the same as separating the direct wave from the scattered waves, because C_s^S still includes interac-

tions between the direct waves and the scattered waves, that is, it does not only represent the coda but also includes the terms $\Psi_{x0}\Psi_{ys}^*$ and $\Psi_{xs}\Psi_{y0}^*$).

Perhaps surprisingly, the configurational average of the cross-spectrum of the scattered wavefield decays significantly (Fig. 5c). This observation agrees with Foldy’s result for the configurational average of the autocorrelation (the configurational average of the cross-correlation at $r_{xy} = 0$ is simply the configurational average of the autocorrelation). Foldy derives explicitly that the configurational average of the autocorrelation is larger than the autocorrelation of the configurational average and provides an exhaustive physical interpretation. The difference can be interpreted considering the interference between different wave arrivals, which, in general, reduces $|\Psi|$. Similarly, interference between wave arrivals associated with different scatterer configurations has the result that $|\langle\Psi\rangle|^2$ is, in general, less than $\langle|\Psi|^2\rangle$. For consistency with the next two experiments, we also plotted the analytical solution for the expected cross-spectrum in a uniformly illuminated, strongly heterogeneous medium, that is, expression (25) (with $\alpha = 0.075/\lambda_0$), in Fig. 5(c).

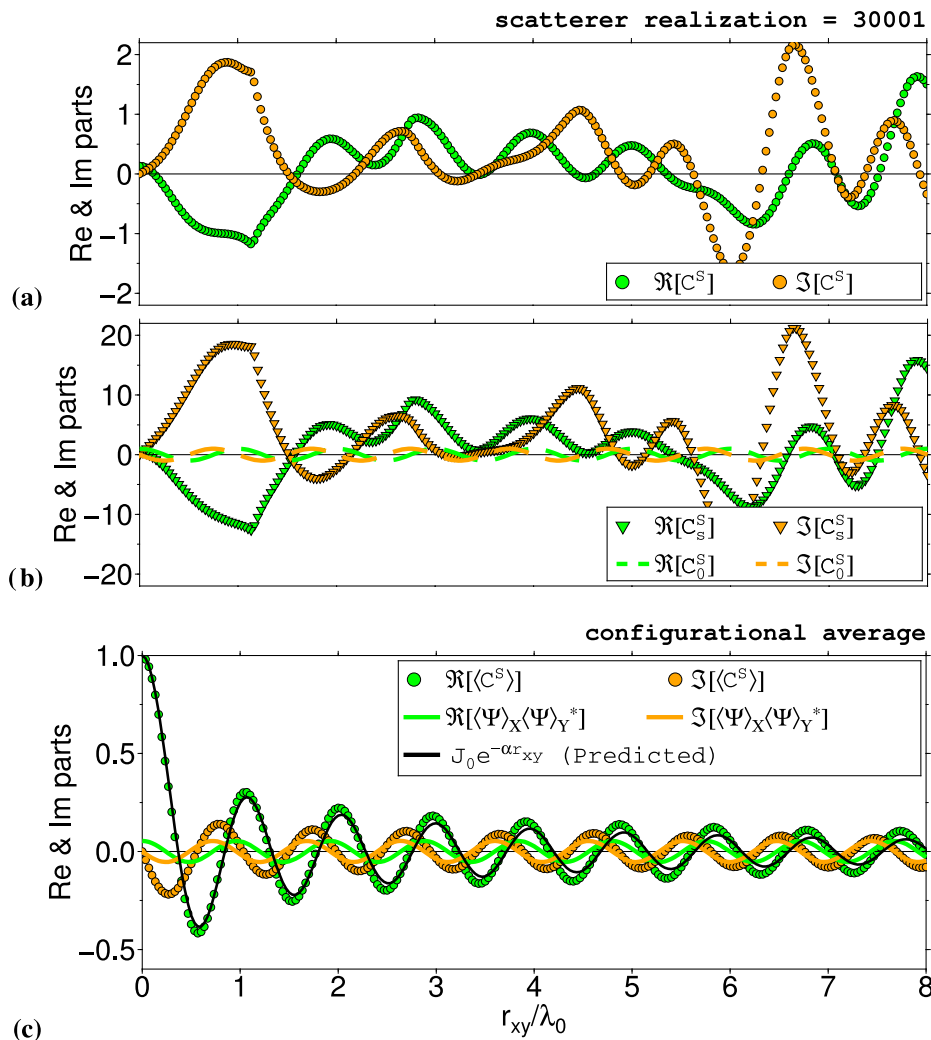


Figure 5. Experiment 1: the cross-spectrum as a function of distance in the scattered wavefield. The cross-spectrum associated with a single configuration of the scatterers is presented in (a). The green and orange dots depict the real and imaginary part of the spectrum, respectively. The cross-correlation of the direct wave, that is, C_0^S , (dashed lines) and its complementary part C_s^S (triangles) are presented in (b). Graph (c) shows the configurationally averaged cross-spectrum obtained from our numerical experiment (dots). For comparison, the cross-spectrum of the configurationally averaged spectrum is plotted (solid lines). Furthermore, the analytical behaviour of $\langle C^S \rangle$ associated with a uniform illuminating wavefield, that is, eq. (25), is depicted in (c) by the solid black line.

4.2 Experiment 2: uniform illumination from all angles

We illuminate the scatterers and receivers prescribing an illumination pattern with a constant power as function of azimuth ($P(\theta) = 1/2\pi$). To decrease computational costs, we evaluate the cross-spectrum up to a maximum receiver separation of $\sim 5.3\lambda_0$. Receiver separation is again incremented by $\lambda_0/30$ (Fig. 2b). For an arbitrarily chosen scattering realization, the cross-spectrum is presented in Fig. 6(a). The imaginary part of the cross-spectrum is zero for all r_{xy} , which agrees with the theory applicable to the setup of this experiment, that is, eq. (18).

As in Fig. 5, we have isolated the cross-correlation of the direct wave and plotted it along with its complementary part (Fig. 6b). We have again normalized both $C_0^S(r_{xy})$ and $C_s^S(r_{xy})$ with respect to $C_0^S(r_{xy} = 0)$. Contrary to the cross-spectrum associated with a single incident wave, C_s^S does not dominate the behaviour of C^S : we observe that C_0^S and C_s^S contribute approximately equally to the behaviour of the cross-spectrum. This reduction in the relative strength of C_s^S can be explained by the isotropic illumination of the scatterers. In accordance with theory, that is, $C^S \propto \Im[G(r_{xy})]$,

spurious arrivals vanish. This has been shown explicitly for both single scattered waves (Snieder *et al.* 2008) and multiple scattered waves (Snieder & Fleury 2010). Compared to our first experiment, the absence of spurious arrivals in C_s^S causes an amplitude reduction with respect to C_0^S . For that reason, C_s^S leaves a significantly lower imprint on the behaviour of C^S for an isotropic distribution of sources. Thanks to this cancellation of spurious arrivals we only need to average over 768 scattering realizations to obtain a stable estimate of the configurationally averaged cross-spectrum (compared to 38400 for illumination by a single plane wave). Fig. 6(c) shows that this configurationally averaged cross-spectrum, that is, the numerically simulated $\Re[\langle C^S \rangle]$, coincides with expression (25). We have normalized $\langle C^S \rangle$ with respect to $\langle C^S(r_{xy} = 0) \rangle$. For comparison, we have plotted the analytical solution for the cross-spectrum in a uniformly illuminated, dissipative medium (C^D with $a_m = 0$ for $m > 0$ and $a_0 = 1/2\pi$). Our experiment confirms that the configurationally averaged cross-spectrum $\langle C^S \rangle$ decays faster than C^D : $J_0(\omega r_{xy}/c) e^{-\alpha r_{xy}}$ (with $\alpha = 0.075/\lambda_0$) versus $J_0(\omega r_{xy}/c)$, respectively.

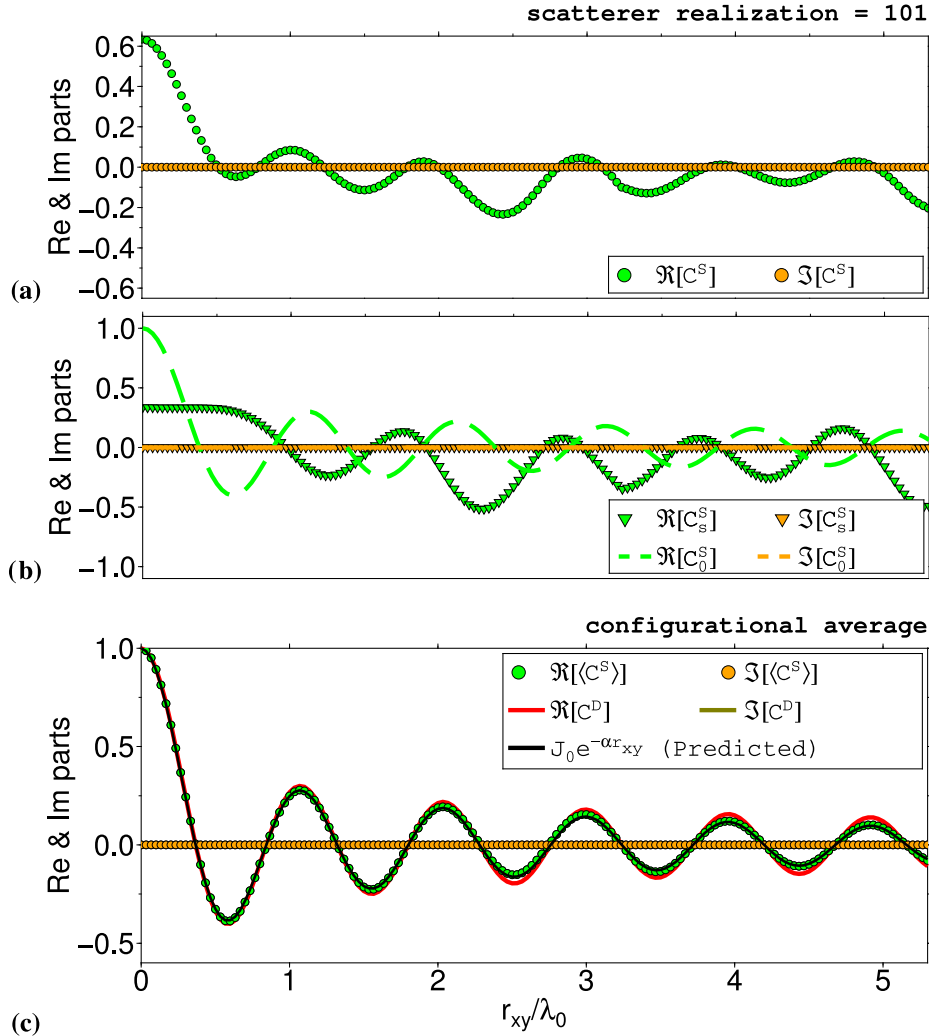


Figure 6. Experiment 2: graphs (a) and (b) present the same quantities as in Fig. 5, but for a wavefield consisting of plane waves incident from all directions with equal power. Graph (c) compares the configurationally averaged cross-spectrum in a scattered wavefield (green and orange dots) to the cross-spectrum associated with a dissipative medium, that is, eq. (5) with $a_m = 0$ for $m > 0$ and $a_0 = 1/2\pi$ (solid red and dark yellow lines). The numerically computed $\Re[C^S]$ coincides with theory, that is, eq. (25) (depicted by the solid black line).

We investigate the impact of the spectral whitening procedure on the amplitudes. Fig. 7 presents the numerically obtained $\langle \rho_S \rangle$ and compares it to ρ_D . The figure bears a striking resemblance to Fig. 6(c) for two reasons. First, the attenuation of ρ_D , given by expression (9) (with $a_m = 0$ for $m > 0$ and $a_0 = 1/2\pi$), is negligible with respect to the attenuation of C^D (a factor $1/I_0(0.075r_{xy}/\lambda_0)$ versus 1, respectively), which makes their behaviour very alike. Secondly, $\langle \rho_S \rangle$ appears to decay at an equal rate as $\langle C^S \rangle$, that is, $e^{-\alpha r_{xy}}$. We cannot prove such equality analytically, but their similar behaviour can be understood intuitively by considering Foldy's result for the expected value of the autocorrelation in relation to the illumination considered. Given the uniform illumination considered here, $\langle |\Psi|^2 \rangle$ can be expected equal for all receivers. Furthermore, the loss of coherency, which depends on $\nu \langle F \rangle$ and is approximated by eq. (23), can be due to either few strong scatterers or many weak scatterers (Fig. 3a). On the one hand, in case of few strong scatterers, the deviation of a single scattering realization from the configurational average can be expected to be large and many scattering realizations will be needed to converge to the expected values of C^S and $|\Psi|^2$. On the other hand, in the limit of an infinite number of isotropic point scatterers with their scattering amplitudes approach-

ing zero, each scattering realization's $|\Psi|^2$ will approach $\langle |\Psi|^2 \rangle$. In the latter case, the division by $\sqrt{C_{xx}^S} \sqrt{C_{yy}^S}$ in eq. (17) may not change the decay of $\langle \rho_S \rangle$ with respect to the decay of $\langle C^S \rangle$. This in turn suggests that $\langle \rho_S \rangle \propto \langle C^S \rangle$ in this limit. An exponential decay of $\langle \rho_S \rangle$ agrees with the findings of Lin *et al.* (2011).

4.3 Experiment 3: non-uniform illumination

In our third experiment we illuminate the assemblages of scatterers with a wavefield characterized by an illumination described by substitution of $a_0 = 1/2\pi$, $a_2 = 1/4\pi$ and $a_3 = 1/5\pi$ in eq. (4); the other coefficients are set to zero. The power of the wavefield as a function of azimuth is shown in Fig. 8. Similar to the previous experiment, we evaluate the cross-spectrum up to a maximum receiver separation of $\sim 5.3\lambda_0$ and increment the separation of the receivers by $\lambda_0/30$. We average over a total of 1536 scattering realizations to estimate the configurationally averaged cross-spectrum. With respect to the previous experiment, twice as many realizations are thus needed before the numerically simulated averaged cross-spectrum converges to its theoretical values. This can be attributed

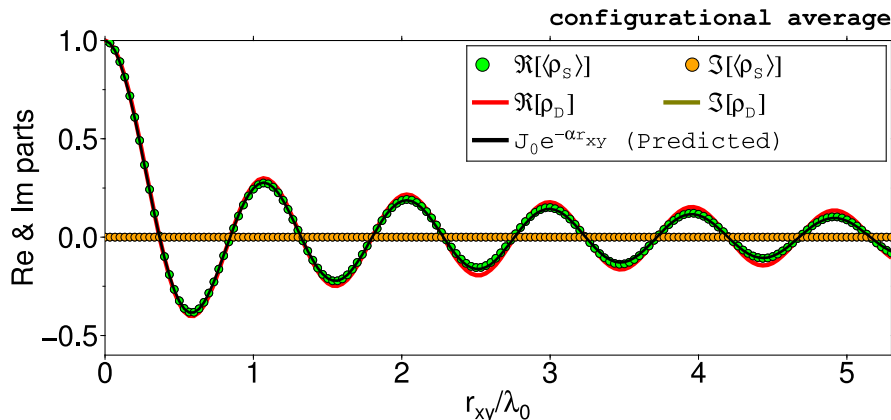


Figure 7. Experiment 2: the configurationally averaged coherency in a scattered wavefield (green and orange dots) compared to the coherency in a dissipative medium, that is, eq. (5) (solid red and dark yellow lines; the latter is overprinted by the orange dots). For comparison, the predicted behaviour of $\Re\{\langle C^S \rangle\}$, that is, according to eq. (25), is plotted on top (solid black line).

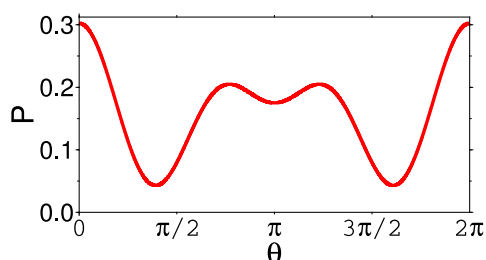


Figure 8. The power of the illuminating wavefield is defined by $a_0 = 1/2\pi$, $a_2 = 1/4\pi$ and $a_3 = 1/5\pi$. The cross-spectra resulting from such an illumination pattern are shown in Fig. 9.

to the lack of complete cancellation of the spurious arrivals due to the non-uniform illumination pattern (Snieder *et al.* 2008; Snieder & Fleury 2010).

The configurationally averaged cross-spectrum and configurationally averaged coherency are presented in Fig. 9. We observe a relatively large difference between the behaviour of $\langle C^S \rangle$ and C^D (Fig. 9a); each associated with a different attenuation mechanism. The relatively large amplitude deviation of C^D from its behaviour associated with a uniform illumination (Fig. 6c) cannot be observed for $\langle C^S \rangle$. In fact, the observed amplitude of $\langle C^S \rangle$ is quite close to its behaviour in our previous experiment and hence quite close to the behaviour of the right-hand side of (25). Also, while the imaginary part of C^D is clearly oscillating, $\Im\{\langle C^S \rangle\}$ has a maximum amplitude only slightly larger than zero. This indicates that, despite the non-uniformity of the wavefield, the spurious arrivals cancel to a great extent for the illumination considered here. Finally, the phase of the symmetric part of the cross-correlation, that is, $\Re\{\langle C^S \rangle\}$, is largely unaffected by the non-uniformity of $P(\theta)$. This suggests that phase velocity measurements may give results that only slightly deviate from the ‘real’ phase velocity and is in line with the data analyses by Gouéard *et al.* (2008) and Froment *et al.* (2010).

The behaviour of the coherency (Fig. 9b) is almost coinciding with the behaviour of the cross-spectrum (Fig. 9a); both in a scattered and a dissipative wavefield. Regarding the latter, the stronger decay of ρ_D with respect to C^D is negligible. One should understand, however, that this difference in decay between ρ_D and C^D is subject to significant change when sources are located closer to the receivers (Tsai 2011). Also, the spectral whitening does not seem to affect the behaviour of the cross-spectrum, that is, $\langle \rho_S \rangle$ exhibits the same behaviour as $\langle C^S \rangle$. Most likely, this can be explained by the

arguments given at the end of Section 4.2; the observed similarity in behaviour may hence not hold for sparse distributions of rather strong scatterers. In the following section we relate the results in this and previous sections to recent studies focusing on the attenuation of the ambient seismic field by means of a simple example.

5 THE AZIMUTHALLY AND SPATIALLY AVERAGED COHERENCY

In this section we relate our findings to the EBF method. Ultimately, in the context of scattering due to isotropic point scatterers, averaging complex coherencies associated with a single receiver pair over different scattering realizations is the same as averaging complex coherencies associated with a specific scattering region over different equally separated receiver pairs within that region; provided, of course, that the scattering region has a constant or close to constant $\nu(F)$. Additionally, applied to our idealized point scattering model, that region is required to have a homogeneous background medium.

We exemplify this analogy between the EBF method and averaging over different scattering realizations by generating an (arbitrary) array of receiver locations in the northwestern USA (Yellowstone area; Fig. 10, left). The array consists of a rather large number of receivers which allows us to average the coherency over sufficient receiver pairs. We consider a background wavelength $\lambda_0 = 40.8$ km due to incident waves with periods of 12 s that propagate with a velocity of 3.4 km s⁻¹. Furthermore, we assume uniform illumination from all angles and prescribe ν independent of location which implies a constant k_{eff} . We compute the wavefield 20 times, each time incrementing ν by 1.912×10^{-3} km⁻². To make the example more realistic, we allow for scatterers with different scattering amplitudes. The probability of a scatterer’s strength, that is, $|f|$, is described by,

$$p_f(f, \mu, s) = \frac{1}{p_f} \left[1 + \cos\left(\frac{|f| - \mu}{s} \pi\right) \right], \quad (26)$$

where μ denotes the mean scatterer strength and p_f is supported between $|f| = \mu - s$ and $|f| = \mu + s$; the normalization constant p_f ensures that $\int p_f df = 1$. In Appendix C we show how $\langle F \rangle$ can be written explicitly in terms of μ and s . We set $\mu = 0.30$ and $s = 0.15$ and use eq. (C5) to compute the expected scattering amplitude. Given a certain scatterer density ν , the expected attenuation rate and phase velocity can be computed by eqs (14) and (13) through eq. (12). The right map in Fig. 10 illustrates the randomly generated

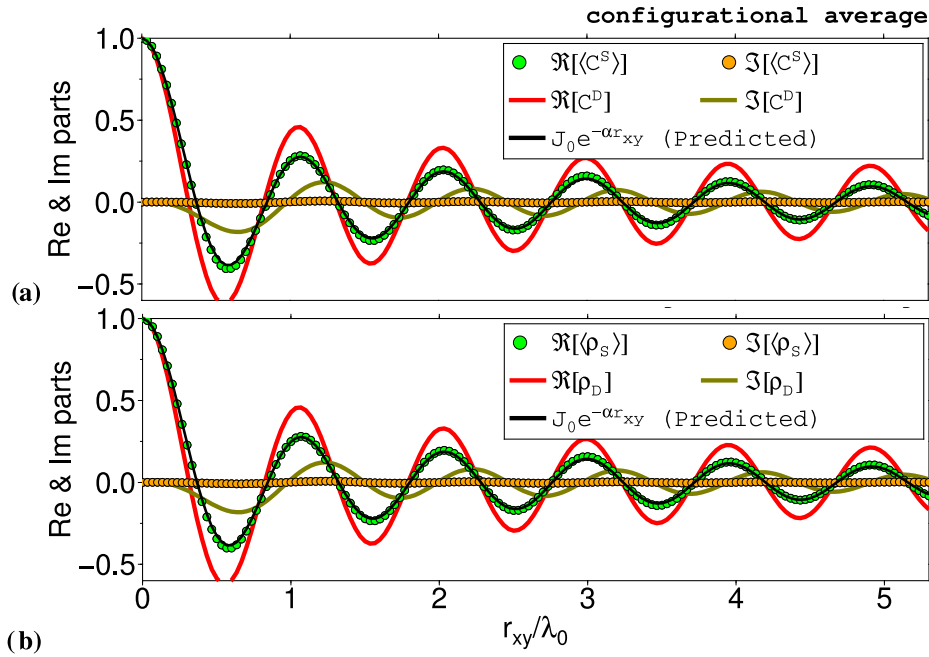


Figure 9. Experiment 3: the configurationally averaged cross-spectrum in a scattered wavefield (green and orange dots) is compared to the cross-spectrum in a dissipative medium, that is, eq. (5) (solid red and dark yellow lines) in (a). In (b) we make the same comparison for the coherency. The analytical behaviour of $\langle C^S \rangle$ associated with a uniform illuminating wavefield, that is, eq. (25), is depicted (in both (a) and (b)) by the solid black line.

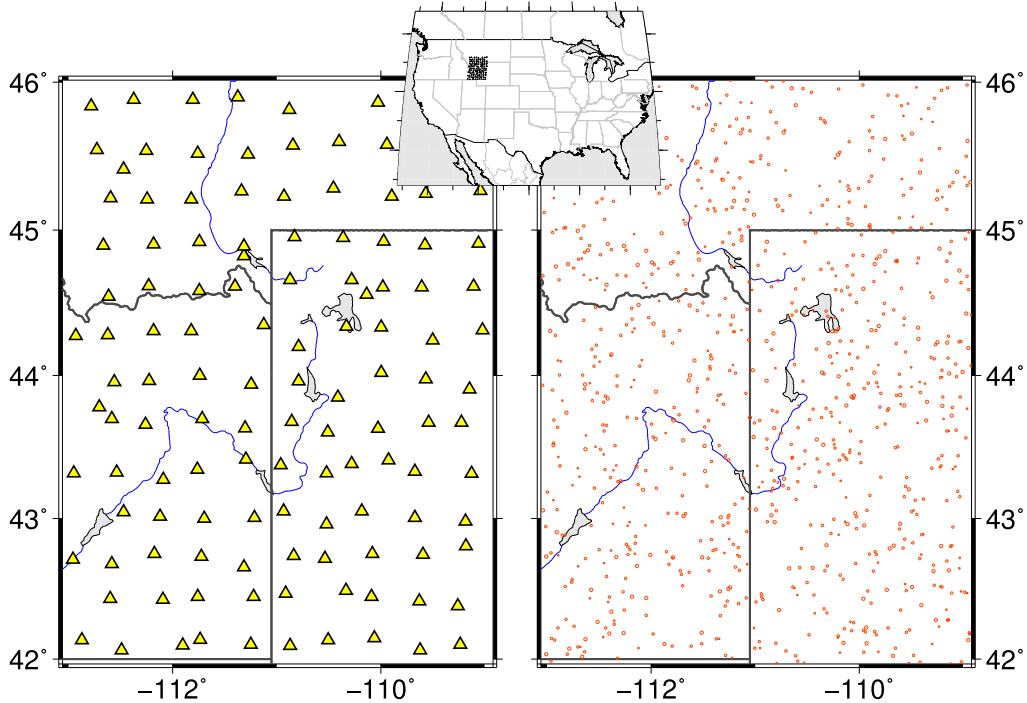


Figure 10. Receiver locations at which the ambient wavefield is computed (left) and randomly generated scatterer locations and strengths (given by the size of the circles) for a prescribed scatterer density of 5.74×10^{-3} scatterers km^{-2} (right). The measured decay and phase velocity of the spatially and azimuthally averaged coherency associated with this scatterer density is depicted in Fig. 11 by the red marked green dot.

scatterer locations and strengths for a prescribed scatterer density of 5.74×10^{-3} scatterers km^{-2} .

In line with earlier studies (Lawrence & Prieto 2011; Weemstra *et al.* 2013), we introduce the binned spatially and azimuthally averaged coherency, denoted $\bar{\rho}_S$. We discretize distance in bins with

width w and enumerate the bins by giving them indices $i = 1, 2, \dots, N$. The centre distance of a bin with index i is denoted by r_i and the number of receiver pairs whose receiver–receiver distance r fulfills the criterion $[r_i - (w/2)] \leq r < [r_i + (w/2)]$ is denoted by M_i . After assigning each receiver pair to the appropriate bin, the

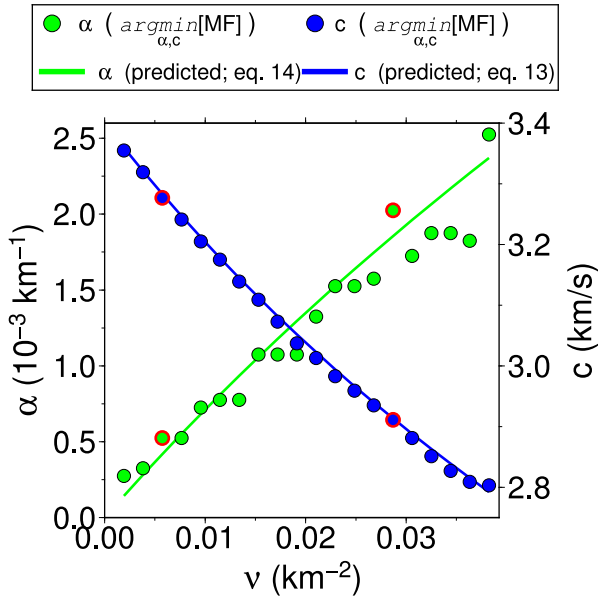


Figure 11. Comparison between the attenuation rate and phase velocity retrieved through our inversion for α and c by minimizing (28) (green and blue dots, respectively) and the predicted attenuation rate and phase velocity according to eqs (23) and (24) (green and blue solid lines, respectively). The red circled dots correspond to the azimuthally and spatially averaged complex coherencies presented in Fig. 12.

binned spatially and azimuthally averaged coherency is computed by,

$$\bar{\rho}_S(r_i) \equiv \frac{1}{M_i} \sum_{j=1}^{M_i} \rho_{S_j}, \quad (27)$$

where for each bin the summation is over the total number of receiver pairs it contains, that is, M_i , and where ρ_{S_j} denotes the coherency associated with receiver pair j . Similar to the previously mentioned data analysis papers, we determine the decay of the real part of the spatially and azimuthally averaged coherency by fitting an exponentially decaying Bessel function. We introduce the misfit function

$$\text{MF}(\alpha, c) = \sum_{i=1}^N \left| \Re[\bar{\rho}_S(r_i)] - J_0\left(\frac{r_i \omega}{c}\right) e^{-\alpha r_i} \right|. \quad (28)$$

We use a bin width of $w = \lambda/25 \approx 1.64$ km and only consider $\bar{\rho}_S$ associated with bins that fulfill the criterion $\lambda < r_i < 6\lambda$ while averaging the complex coherencies from different receiver pairs. The fact that MF is based on the L1-norm, mitigates the effect of outliers due to limited numbers of receiver pairs in some bins.

The attenuation rates and phase velocities estimated by the minima of (28) are compared to the theoretically predicted expected attenuation rates and expected phase velocities for $\langle C^S \rangle$ in Fig. 11. Since we have assumed uniform illumination from all angles, these predicted values are simply given by eqs (23) and (24) (with F computed using eq. (C5)). As expected, the estimated values follow the same trend as the analytical curves and especially the phase velocity is well constrained. We observe that the attenuation rate estimates deviate more from the analytical predictions for higher scatterer densities. This can be explained by the higher deviation of individual realizations from their expected values for higher scat-

terer densities. Fig. 12 illustrates this effect: averages of ρ_S associated with individual bins exhibit a larger variation in Fig. 12(b), which presents $\bar{\rho}_S(r_i)$ for a relatively high scatterer density. Note that the imaginary parts are zero due to the uniform illumination and the relation associated with this illumination pattern, that is, eq. (25).

6 DISCUSSION AND CONCLUSION

Previous studies have emphasized the dependence of the amplitude of the cross-correlation on the distribution of sources in a dissipative medium (Tsai 2011; Hanasoge 2013). Our results show that multiple scattering mitigates the effect of the source distribution on the amplitude of the cross-correlation; this has been shown for the phase of the cross-correlation previously (Froment *et al.* 2010; Sens-Schönfelder & Wegler 2011). Specifically, we show that the spatially and azimuthally averaged cross-spectrum decays exponentially in case of a purely elastic scattering medium illuminated uniformly from all angles. Compared to intrinsic attenuation, successful recovery of scattering attenuation is therefore feasible under relaxed constraints: the excitation of noise is not required to be uniform (Tsai 2011; Nakahara 2012), but merely such that the resulting illumination pattern is uniform.

A few caveats apply while translating our results for distributions of isotropic point scatterers to data studies aiming to recover subsurface attenuation using interferometric surface waves. First, in case of abrupt changes in either scatterer density or strength, the effective wavenumber changes accordingly and the azimuthal and spatial averaging may produce unexpected or meaningless results. Second and somewhat related, it is important that the typical length scale over which the scattering properties of the medium vary, is larger than the size of the regions over which cross-spectra are averaged. This remark also applies to dissipative media however: the assumption that phase velocity and attenuation are laterally invariant throughout the region over which coherency measurements are averaged, should not be violated (Tsai 2011). In fact, the recent analysis by Menon *et al.* (2014) reveals that spatial and azimuthal averaging may result in significant apparent attenuation in case of an anisotropic velocity medium. A third caveat concerns the trade-off between scatterer density and scattering amplitudes: loss of coherency can be due to either few strong scatterers or many weak scatterers (see Fig. 3a). A region with few strong heterogeneities, however, may well require an unreasonably high number of individual coherency measurements, that is, receiver pairs, to obtain a ‘stable’ measure of the coherency. Finally, the assumption of waves having a single velocity corresponding to one frequency does not hold in a layered Earth: several modes may be observed at one frequency (Aki & Richards 2002; Weemstra *et al.* 2013). In practice, ambient vibrations associated with primary microseisms (0.05–0.1 Hz) are usually dominated by fundamental-mode waves, whereas secondary microseisms (0.1–0.2 Hz) may well contain significant overtone energy (Kimmman *et al.* 2012; Menon *et al.* 2014).

Considering the caveats listed above and the assumptions made in this work, we want to stress that with the experiments, analytical relations and example presented in this paper we do not want to claim that the method introduced by Prieto *et al.* (2009) enables one to recover the ‘true’ subsurface attenuation. Ultimately, a purely elastic scattering medium is a rather extreme assumption and applied to surface waves on Earth may in many cases not be very realistic. The assumption of a purely homogenous dissipative subsurface

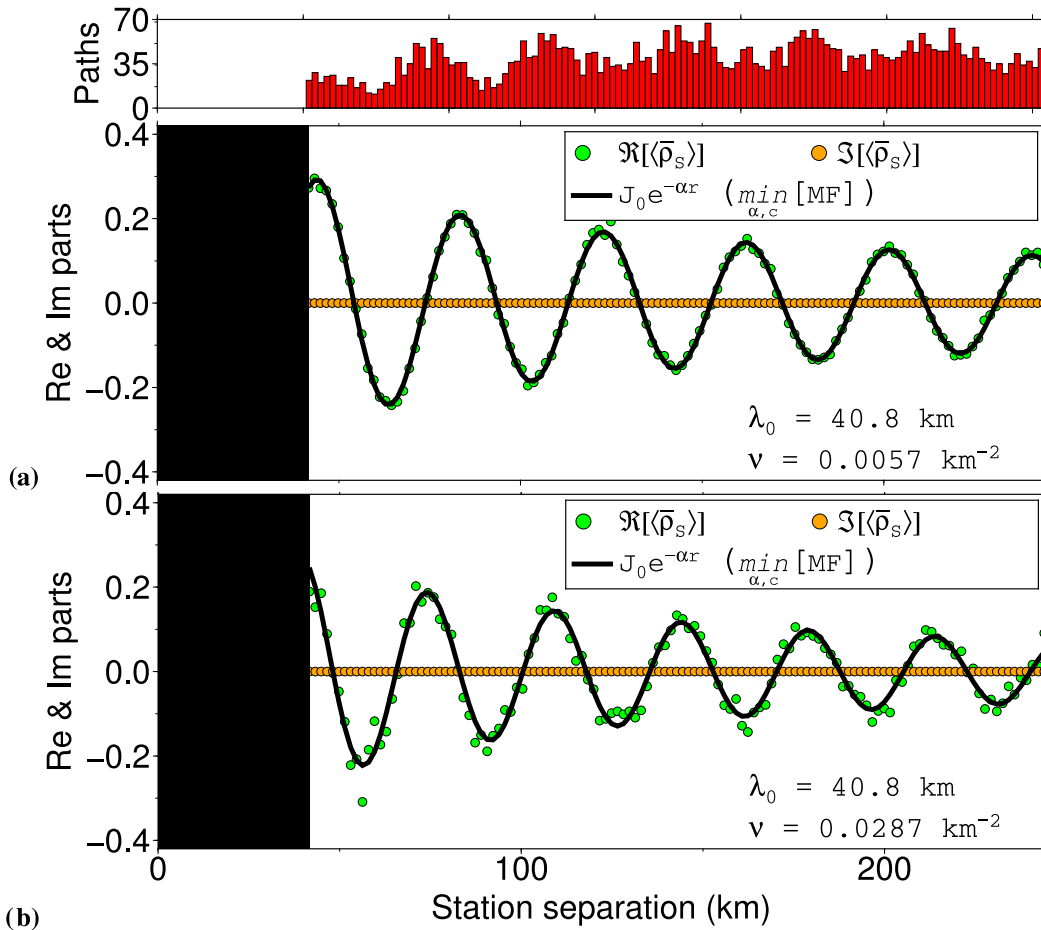


Figure 12. Spatially and azimuthally averaged coherency ($\bar{\rho}_S(r_i)$; green and orange dots) computed from the receiver configuration shown in Fig. 10. An ambient-seismic waveform characterized by uncorrelated equal amplitude waves arriving from all directions is assumed. Plots (a) and (b) are associated with scatterer densities of 5.74×10^{-3} and 28.7×10^{-3} scatterers km^{-2} , respectively. Scatterers vary in strength according to eq. (26) with μ and s set to 0.30 and 0.15, respectively. The exponentially decaying Bessel function that minimizes eq. (28) is given by the black solid line. Receiver pairs separated by less than 1 wavelength or more than 6 wavelengths are discarded.

made in some recent theoretical studies (e.g. Tsai 2011; Weaver 2012), however, may well be equally unrealistic in other cases. Our results therefore do suggest that for some regions the decay of the (whitened) cross-spectrum may well be more sensitive to local structure than suggested in previous studies (Tsai 2011; Hanasoge 2013).

The following conclusions, applicable to 2-D media illuminated by far-field sources, can be drawn. First, the decay of a single wave propagating through a dissipative medium and the decay of the configurational average of a single wave propagating through a scattering medium coincide in case the complex wavenumbers describing the two media coincide. In that case, however, the cross-spectra do not coincide; specifically, the real part of the cross-spectrum in the scattering medium exhibits significant decay (illustrated by experiment 1). Second, the decay of the cross-spectrum in a uniformly illuminated dissipative homogeneous medium and the decay of the configurationally averaged cross-spectrum in a uniformly illuminated non-dissipative scattering medium, described by coinciding complex wavenumbers, do not coincide. In fact, the configurationally averaged cross-spectrum in a uniformly illuminated scattering medium coincides with a Bessel function multiplied by an exponentially decaying term (eq. 25), whereas the cross-spectrum in a dissipative medium is described by only a Bessel

function (eq. 5 with $a_m = 0$ for $m > 0$) (illustrated by experiment 2). Third, the presence of scatterers mitigates the deviation of the coherency due to a non-uniform illumination pattern from its behaviour due to uniform illumination pattern (illustrated by experiment 3). Finally, provided a regionally constant (or smooth) scatterer density, azimuthal and spatial averaging of cross-spectra computed from equidistant receiver pairs is equivalent to averaging over different scatterer ensembles characterized by equal scatterer densities.

ACKNOWLEDGEMENTS

We gratefully acknowledge support from the QUEST Initial Training Network funded within the EU Marie Curie actions programme. CW is supported by the Netherlands Research Centre for Integrated Solid Earth Science (ISES). The authors warmly thank Xin Liu and one anonymous referee for their considerable help in improving the manuscript. This study benefitted from interactions with Victor Tsai, Stewart Greenhalgh and Filippo Broggin. We would like to thank Max Rietmann and Dave May for advising us on parallel computing. Part of the figures were generated with the help of Generic Mapping Tools (Wessel & Smith 1991).

REFERENCES

- Abramowitz, M. & Stegun, I.A., 1964. *Handbook of Mathematical Functions with Formulas, Graphs, and Mathematical Tables*, National Bureau of Standards Applied Mathematics Series, New York.
- Aki, K., 1957. Space and time spectra of stationary stochastic waves, with special reference to microtremors, *Bull. Earthq. Res. Inst., Univ. Tokyo*, **35**, 415–457.
- Aki, K. & Richards, P.G., 2002. *Quantitative Seismology*, 2nd edn, University Science Books.
- Boschi, L., Weemstra, C., Verbeke, J., Ekstrom, G., Zunino, A. & Giardini, D., 2013. On measuring surface wave phase velocity from station-station cross-correlation of ambient signal, *Geophys. J. Int.*, **192**(1), 346–358.
- Campillo, M. & Paul, A., 2003. Long-range correlations in the diffuse seismic coda, *Science*, **299**(5606), 547–549.
- Cox, H., 1973. Spatial correlation in arbitrary noise fields with application to ambient sea noise, *J. acoust. Soc. Am.*, **54**(5), 1289–1301.
- Duvall, T.L., Jefferies, S.M., Harvey, J.W. & Pomerantz, M.A., 1993. Time-distance helioseismology, *Nature*, **362**(6419), 430–432.
- Foldy, L.L., 1945. The multiple scattering of waves 1. General theory of isotropic scattering by randomly distributed scatterers, *Phys. Rev.*, **67**(3–4), 107–119.
- Froment, B., Campillo, M., Roux, P., Gouédard, P., Verdel, A. & Weaver, R.L., 2010. Estimation of the effect of nonisotropically distributed energy on the apparent arrival time in correlations, *Geophysics*, **75**(5), SA85–SA93.
- Godin, O.A., Zobin, N.A. & Goncharov, V.V., 2010. Ocean tomography with acoustic daylight, *Geophys. Res. Lett.*, **37**(13), L13605, doi:10.1029/2010GL043623.
- Gouédard, P., Roux, P., Campillo, M. & Verdel, A., 2008. Convergence of the two-point correlation function toward the Greens function in the context of a seismic-prospecting data set, *Geophysics*, **73**(6), V47–V53.
- Groenenboom, J. & Snieder, R., 1995. Attenuation, dispersion, and anisotropy by multiple scattering of transmitted waves through distributions of scatterers, *J. acoust. Soc. Am.*, **98**(6), 3482–3492.
- Groos, J.C. & Ritter, J.R.R., 2009. Time domain classification and quantification of seismic noise in an urban environment, *Geophys. J. Int.*, **179**(2), 1213–1231.
- Hanasoge, S.M., 2013. The influence of noise sources on cross-correlation amplitudes, *Geophys. J. Int.*, **192**(1), 295–309.
- Haney, M.M., 2009. Infrasonic ambient noise interferometry from correlations of microbaroms, *Geophys. Res. Lett.*, **36**(19), L19808, doi:10.1029/2009GL040179.
- Harmon, N., Rychert, C. & Gerstoft, P., 2010. Distribution of noise sources for seismic interferometry, *Geophys. J. Int.*, **183**(3), 1470–1484.
- Hasselman, K., 1963. A statistical analysis of the generation of microseisms, *Rev. Geophys.*, **1**(2), 177–210.
- Kimman, W.P., Campman, X. & Trampert, J., 2012. Characteristics of seismic noise: fundamental and higher mode energy observed in the northeast of the Netherlands, *Bull. seism. Soc. Am.*, **102**(4), 1388–1399.
- Kohler, M.D., Heaton, T.H. & Bradford, S.C., 2007. Propagating waves in the steel, moment-frame factor building recorded during earthquakes, *Bull. seism. Soc. Am.*, **97**(4), 1334–1345.
- Lawrence, J.F. & Prieto, G.A., 2011. Attenuation tomography of the western United States from ambient seismic noise, *J. geophys. Res.*, **116**(B6), B06302, doi:10.1029/2010JB007836.
- Lax, M., 1951. Multiple scattering of waves, *Rev. Mod. Phys.*, **23**(4), 287–310.
- Lin, F.-C., Ritzwoller, M.H. & Shen, W., 2011. On the reliability of attenuation measurements from ambient noise cross-correlations, *Geophys. Res. Lett.*, **38**(11), L11303, doi:10.1029/2011GL047366.
- Liu, X. & Ben-Zion, Y., 2013. Theoretical and numerical results on effects of attenuation on correlation functions of ambient seismic noise, *Geophys. J. Int.*, **194**, 1966–1983.
- Longuet-Higgins, M.S., 1950. A theory of the origin of microseisms, *Phil. Trans. R. Soc. Lond., A, Math. Phys. Sci.*, **243**(857), 1–35.
- Menon, R., Gerstoft, P. & Hodgkiss, W.S., 2014. On the apparent attenuation in the spatial coherence estimated from seismic arrays, *J. geophys. Res.*, **119**(4), 3115–3132.
- Nakahara, H., 2012. Formulation of the spatial autocorrelation (SPAC) method in dissipative media, *Geophys. J. Int.*, **190**(3), 1777–1783.
- Newton, R.G., 1976. Optical theorem and beyond, *Am. J. Phys.*, **44**(7), 639–642.
- Newton, R.G., 2002. *Scattering Theory of Waves and Particles*, Dover Publications Inc.
- Prieto, G.A., Lawrence, J.F. & Beroza, G.C., 2009. Anelastic Earth structure from the coherency of the ambient seismic field, *J. geophys. Res.*, **114**, B07303, doi:10.1029/2008JB006067.
- Roux, P. & Fink, M., 2003. Green's function estimation using secondary sources in a shallow water environment, *J. acoust. Soc. Am.*, **113**(3), 1406–1416.
- Sens-Schönfelder, C. & Wegler, U., 2011. Passive image interferometry for monitoring crustal changes with ambient seismic noise, *C. R. Geosci.*, **343**(8–9), 639–651.
- Shapiro, N.M. & Campillo, M., 2004. Emergence of broadband Rayleigh waves from correlations of the ambient seismic noise, *Geophys. Res. Lett.*, **31**(7), L07614, doi:10.1029/2004GL019491.
- Snieder, R., 1988. Large-scale waveform inversions of surface waves for lateral heterogeneity: 2. Application to surface waves in Europe and the Mediterranean, *J. geophys. Res.*, **93**(B10), 12 067–12 080.
- Snieder, R., 2004. Extracting the Green's function from the correlation of coda waves: a derivation based on stationary phase, *Phys. Rev. E*, **69**(4), doi:10.1103/PhysRevE.69.046610.
- Snieder, R., 2007. Extracting the Green's function of attenuating heterogeneous acoustic media from uncorrelated waves, *J. acoust. Soc. Am.*, **121**(5), 2637–2643.
- Snieder, R. & Fleury, C., 2010. Cancellation of spurious arrivals in Green's function retrieval of multiple scattered waves., *J. acoust. Soc. Am.*, **128**(4), 1598–1605.
- Snieder, R., Wapenaar, K. & Wegler, U., 2007. Unified Green's function retrieval by cross-correlation; connection with energy principles, *Phys. Rev. E*, **75**(3), doi:10.1103/PhysRevE.75.036103.
- Snieder, R., van Wijk, K., Haney, M. & Calvert, R., 2008. Cancellation of spurious arrivals in Green's function extraction and the generalized optical theorem, *Phys. Rev. E*, **78**(3), 036606, doi:10.1103/PhysRevE.78.036606.
- Snieder, R. & Şafak, E., 2006. Extracting the building response using seismic interferometry: theory and application to the Millikan library in Pasadena, California, *Bull. seism. Soc. Am.*, **96**(2), 586–598.
- Strutt, J.W., 1871. XV. On the light from the sky, its polarization and colour, *Lond. Edinb. Dubl. Phil. Mag. J. Sci.*, **41**(271), 107–120.
- Tsai, V.C., 2011. Understanding the amplitudes of noise correlation measurements, *J. geophys. Res.*, **116**, B09311, doi:10.1029/2011JB008483.
- Tsai, V.C. & Moschetti, M.P., 2010. An explicit relationship between time-domain noise correlation and spatial autocorrelation (SPAC) results, *Geophys. J. Int.*, **182**(1), 454–460.
- van De Hulst, H.C., 1949. On the attenuation of plane waves by obstacles of arbitrary size and form, *Physica*, **15**(8–9), 740–746.
- Verbeke, J., Boschi, L., Stehly, L., Kissling, E. & Michelini, A., 2012. High-resolution Rayleigh-wave velocity maps of central Europe from a dense ambient-noise data set, *Geophys. J. Int.*, **188**(3), 1173–1187.
- Wapenaar, K. & Fokkema, J., 2006. Green's function representations for seismic interferometry, *Geophysics*, **71**(4), SI33–SI46.
- Waterman, P.C. & Truell, R., 1961. Multiple scattering of waves, *J. Math. Phys.*, **2**(4), 512–537.
- Weaver, R. & Lobkis, O., 2002. On the emergence of the Green's function in the correlations of a diffuse field: pulse-echo using thermal phonons, *Ultrasonics*, **40**(1–8), 435–439.
- Weaver, R.L., 2012. On the retrieval of attenuation from the azimuthally averaged coherency of a diffuse field, preprint, ([arXiv:1206.6513](https://arxiv.org/abs/1206.6513)).
- Weaver, R.L. & Lobkis, O.I., 2001. Ultrasonics without a source: thermal fluctuation correlations at MHz frequencies, *Phys. Rev. Lett.*, **87**(13), doi:10.1103/PhysRevLett.87.134301.
- Weemstra, C., Boschi, L., Goertz, A. & Artman, B., 2013. Seismic attenuation from recordings of ambient noise, *Geophysics*, **78**(1), Q1–Q14.
- Weemstra, C., Westra, W., Snieder, R. & Boschi, L., 2014. On estimating attenuation from the amplitude of the spectrally whitened ambient seismic field, *Geophys. J. Int.*, **197**(3), 1770–1788.

Wessel, P. & Smith, W., 1991. Free software helps map and display data, *EOS, Trans. Am. geophys. Un.*, **72**, 441–446.
 Wu, R.-S., 1982. Mean field attenuation and amplitude attenuation due to wave scattering, *Wave Motion*, **4**(3), 305–316.
 Wu, R.-S. & Aki, K., 1988. Multiple scattering and energy transfer of seismic waves—separation of scattering effect from intrinsic attenuation:

II. Application of the theory to Hindu Kush region, *Pure appl. Geophys.*, **128**(1–2), 49–80.
 Yokoi, T. & Margaryan, S., 2008. Consistency of the spatial autocorrelation method with seismic interferometry and its consequence, *Geophys. Prospect.*, **56**(3), 435–451.

APPENDIX A: THE SOLUTION OF THE MULTIPLE SCATTERING PROCESS

In general, a scatterer’s radiation pattern is described by its ‘scattering amplitude’, which depends on the direction of propagation of the incoming and scattered wave. Isotropic point scatterers, however, are characterized by a scattering amplitude that is independent of the incident and scattered wave vector. We denote the scattering amplitude of a scatterer at \mathbf{r}_j by f_j .

Consider a background wavefield,

$$\Psi_0(\mathbf{r}) \equiv e^{i\mathbf{k}_0 \cdot \mathbf{r}}, \tag{A1}$$

where the wave vector \mathbf{k}_0 prescribes the direction of propagation and wavelength of the background incident wave (note that $k_0 = |\mathbf{k}_0|$). The wavefield at \mathbf{r} due to scatterers located at \mathbf{r}_j can be written as a summation over their individual contributions (Foldy 1945; Groenenboom & Snieder 1995), that is,

$$\Psi_s(\mathbf{r}) \equiv \sum_{j=1}^N G^{(0)}(\mathbf{r}, \mathbf{r}_j) f_j \Psi(\mathbf{r}_j), \tag{A2}$$

where we sum over a total of N scatterers. $G^{(0)}(\mathbf{r}, \mathbf{r}_j)$ denotes the Green’s function of the background medium.

In two dimensions, the impulse response to the scalar wave equation is given by

$$\begin{aligned} G^{(0)}(\mathbf{r}, \mathbf{r}') &= \frac{-i}{4} H_0^{(2)}(k_0 |\mathbf{r} - \mathbf{r}'|) \\ &\approx \frac{1}{4} \sqrt{\frac{2}{\pi k_0 |\mathbf{r} - \mathbf{r}'|}} e^{-ik_0 |\mathbf{r} - \mathbf{r}'| - i\pi/4} \quad (k_0 |\mathbf{r} - \mathbf{r}'| \gg 1) \end{aligned} \tag{A3}$$

where $H_0^{(2)}$ is a Hankel function of the second kind and zeroth order. A time dependence $e^{i\omega t}$ is assumed and the Green’s function is a solution to the Helmholtz equation with a negative Dirac delta function as forcing function (Wapenaar & Fokkema 2006). The approximation is valid at distances much larger than the wavelength.

The wavefield at any location \mathbf{r} can be obtained by substituting the right-hand side of (A2) for Ψ_s in eq. (10). The summation in (A2), however, requires the wavefield impinging on the scatterers while the wavefield acting at any of these scatterers depends in turn on the waves scattered away from the other scatterers. This mutual dependence can be reformulated by eliminating a scatterer’s own contribution, that is, for the wavefield at the location of the j th scatterer we have,

$$\Psi(\mathbf{r}_j) = \Psi_0(\mathbf{r}_j) + \sum_{\substack{l=1 \\ l \neq j}}^N G^{(0)}(\mathbf{r}_j, \mathbf{r}_l) f_l \Psi(\mathbf{r}_l). \tag{A4}$$

This linear system of equations can be written in matrix notation and solved for the $\Psi(\mathbf{r}_j)$. The obtained solutions take into account all multiple scattering interactions.

We define

$$\Psi \equiv \begin{pmatrix} \Psi(\mathbf{r}_1) \\ \Psi(\mathbf{r}_2) \\ \dots \\ \Psi(\mathbf{r}_N) \end{pmatrix} \tag{A5}$$

and

$$\Psi_0 \equiv \begin{pmatrix} \Psi_0(\mathbf{r}_1) \\ \Psi_0(\mathbf{r}_2) \\ \dots \\ \Psi_0(\mathbf{r}_N) \end{pmatrix} \tag{A6}$$

and finally the square matrix with rank N ,

$$\mathbf{M} \equiv \begin{pmatrix} -1 & f_2 G^{(0)}(\mathbf{r}_1, \mathbf{r}_2) & \dots & \dots & f_N G^{(0)}(\mathbf{r}_1, \mathbf{r}_N) \\ f_1 G^{(0)}(\mathbf{r}_2, \mathbf{r}_1) & -1 & \dots & \dots & \dots \\ \dots & \dots & \dots & \dots & \dots \\ \dots & \dots & \dots & \dots & \dots \\ f_1 G^{(0)}(\mathbf{r}_N, \mathbf{r}_1) & \dots & \dots & \dots & -1 \end{pmatrix}. \quad (\text{A7})$$

In matrix notation eq. (A4) thus reduces to

$$\mathbf{M}\Psi = -\Psi_0, \quad (\text{A8})$$

which can be written as,

$$\Psi = -\mathbf{M}^{-1}\Psi_0 \quad (\text{A9})$$

This system of equations can be solved numerically using, for example, LU decomposition. In the special case of equal f_j for all scatterers, \mathbf{M} becomes Hermitian and Cholesky decomposition can be used to solve the system, which is approximately twice as fast as LU decomposition. The solutions for the $\Psi(\mathbf{r}_j)$ can be substituted in expression (A2) which enables us to calculate Ψ_s at any location \mathbf{r} . Through eq. (10) we can subsequently calculate the total wavefield at that location.

APPENDIX B: HOW THE OPTICAL THEOREM CAPS THE STRENGTH OF AN ISOTROPIC POINT SCATTERER

Our rather idealized point scatterer does not absorb energy, that is, $\Omega_C = 0$. Conservation of energy therefore equates the total cross-section of a scatterer to its scattering cross-section. Because a scatterer is assumed to be isotropic, its scattering amplitude is independent of the incident and scattered wave vector. Without loss of generality, we position an isotropic point scatterer at the origin, and consider its wavefield as function of distance r away from it, that is,

$$\Psi(r) = G^{(0)}(r) \times f_j \Psi_0(0), \quad (\text{B1})$$

where Ψ_0 is given by eq. (A1). Its outward flux is therefore obtained by:

$$\begin{aligned} \Omega_S &= \int_0^{2\pi} |G^{(0)}(r) \times f \Psi_0(0)|^2 r d\theta \\ &\approx \frac{1}{8k_0\pi} \int_0^{2\pi} |f|^2 d\theta \\ &= \frac{|f|^2}{4k_0}. \end{aligned} \quad (\text{B2})$$

The approximation stems from substitution of the far-field approximation for the Green's function, that is, eq. (A3).

Equating Ω_{TOT} , that is, expression (11), to Ω_S enforces a relation between the real and imaginary part of the scattering amplitude:

$$\Re[f] = \pm \sqrt{-\Im[f](4 + \Im[f])}. \quad (\text{B3})$$

This relation bounds both the imaginary part of f and the maximum amount of energy removed from the incident wave, that is,

$$-4 \leq \Im[f] \leq 0 \quad \text{or} \quad 0 \leq \Omega_{\text{TOT}} \leq 4/k_0. \quad (\text{B4})$$

The optical theorem therefore caps the strength of the isotropic point scatterers.

APPENDIX C: THE EXPECTED SCATTERING AMPLITUDE

The expected scattering amplitude $\langle F \rangle$ can be obtained by solving the integral in eq. (15). Furthermore, in Appendix B we show that conservations of energy constrains the scattering amplitude of an isotropic point scatterer to the contour in the complex plane described $(\Re[f])^2 + (\Im[f] + 2)^2 = 4$. The integral can therefore be computed by evaluating the integrand p_f along this contour. We parametrize the contour by the angle ϕ , which gives $f = 2e^{i(\phi + \pi/2)} - 2i$ and $f = 2e^{i(-\phi + \pi/2)} - 2i$ for negative and positive $\Re[f]$, respectively (see Fig. C1). The expected scattering amplitude is obtained by integration over t from 0 to π ,

$$\langle F \rangle = \begin{cases} \int_0^\pi p_f(\phi) (2e^{i(\phi + \pi/2)} - 2i) d\phi, & \Re[f] = -\sqrt{-\Im[f](4 + \Im[f])} \\ \int_0^\pi p_f(\phi) (2e^{i(-\phi + \pi/2)} - 2i) d\phi, & \Re[f] = \sqrt{-\Im[f](4 + \Im[f])}, \end{cases} \quad (\text{C1})$$

where p_f becomes ϕ -dependent by substituting the appropriate parametrization for f (i.e. $f = 2e^{i(\phi + \pi/2)} - 2i$ and $f = 2e^{i(-\phi + \pi/2)} - 2i$ for negative and positive $\Re[f]$, respectively).

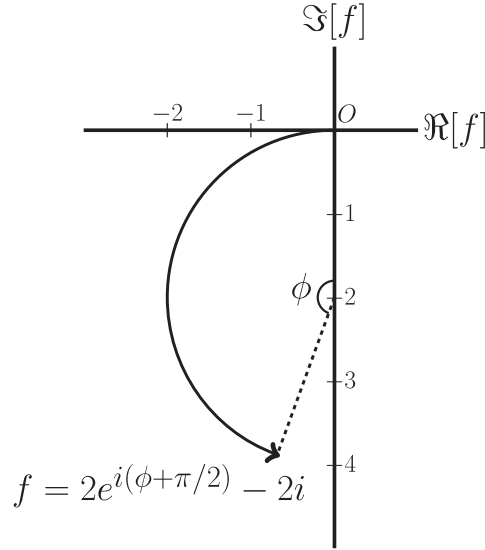


Figure C1. Parametrization of f by $f = 2e^{i(\phi + \pi/2)} - 2i$. The contour associated with positive $\Re[f]$ is not depicted, but is simply obtained by mirroring with respect to the imaginary axis.

We now show how $\langle F \rangle$ can be computed in case the absolute scattering amplitudes are drawn from a raised cosine distribution (eq. 26). We only evaluate the integral associated with negative $\Re[f]$ and relate the result of this evaluation to positive $\Re[f]$ at the end of this appendix. Substituting eq. (26) into eq. (C1) and explicitly writing $f = 2e^{i(\phi + \pi/2)} - 2i$ we have,

$$\langle F \rangle = \frac{1}{p_f^T} \int_{\phi_1}^{\phi_2} \left[1 + \cos \left(\frac{|2e^{i(\phi + \pi/2)} - 2i| - \mu}{s} \pi \right) \right] (2e^{i(\phi + \pi/2)} - 2i) d\phi \tag{C2}$$

where ϕ_1 and ϕ_2 are the angles corresponding to $|f| = \mu - s$ and $|f| = \mu + s$, respectively.

The absolute value of f , in terms of ϕ , can be written as

$$\begin{aligned} |2e^{i(\phi + \pi/2)} - 2i| &= \sqrt{(2e^{i(\phi + \pi/2)} - 2i)(2e^{i(\phi + \pi/2)} - 2i)^*} \\ &= \sqrt{8 - 8 \cos(\phi)}. \end{aligned} \tag{C3}$$

Inverting for ϕ gives,

$$\phi = \cos^{-1} \left(1 - \frac{|f|^2}{8} \right), \tag{C4}$$

which implies that the integration boundaries ϕ_1 and ϕ_2 are given by $\cos^{-1} \left(1 - \frac{(\mu - s)^2}{8} \right)$ and $\cos^{-1} \left(1 - \frac{(\mu + s)^2}{8} \right)$, respectively. Substituting eq. (C3) in eq. (C2) yields,

$$\langle F \rangle = \frac{1}{p_f^T} \int_{\phi_1}^{\phi_2} \left[1 + \cos \left(\frac{\sqrt{8 - 8 \cos(\phi)} - \mu}{s} \pi \right) \right] (2e^{i(\phi + \pi/2)} - 2i) d\phi, \tag{C5}$$

where the normalization factor is defined as

$$p_f^T \equiv \int_{\phi_1}^{\phi_2} \left[1 + \cos \left(\frac{\sqrt{8 - 8 \cos(\phi)} - \mu}{s} \pi \right) \right] d\phi \tag{C6}$$

and ensures that $\int p_f df = 1$.

We obtain $\langle F \rangle$ by numerical integration of expression (C5). The expected value of F associated with positive $\Re[f]$ is simply obtained by substituting $(2e^{i(-\phi + \pi/2)} - 2i)$ for $(2e^{i(\phi + \pi/2)} - 2i)$ in eq. (C5).